Active Control of Buckling: Centralized and Decentralized Approaches

by

Natalya Cohen

Submitted to the Department of Electrical Engineering and Computer Science

in Partial Fulfillment of the Requirements for the Degrees of

Bachelor of Science in Electrical Engineering and Computer Science

and Master of Engineering in Electrical Engineering and Computer Science

at the Massachusetts Institute of Technology

May 23, 1996

Author_____
Department of Electrical Engineering and Computer Science
May 23,1996

Certified by_____
Gerald J. Sussman
Matsushita Professor of Electrical Engineering
Thesis Supervisor

Accepted by_____
F. R. Morgenthaler
Chairman, Department Committee on Graduate Theses

Active Control of Buckling: Centralized and Decentralized Approaches

by

Natalya Cohen

Submitted to the
Department of Electrical Engineering and Computer Science

May 23, 1996

in Partial Fulfillment of the Requirements for the Degrees of
Bachelor of Science in Electrical Engineering and Computer Science
and Master of Engineering in Electrical Engineering and Computer Science

Abstract

This thesis examines two different approaches to active buckling control of a compressively-loaded structural element. The phenomenon of buckling is the single most important factor limiting the load-bearing strength of a structure. Active control of buckling allows us to increase the load-bearing capabilities of compressive members, leading to structures that are both stronger and lighter than the passive structures built today.

Traditionally, active structural control has been performed by *centralized* controllers, which assume both the existence of a global model for the system to be controlled, and the availability of global state information. These assumptions fail, however, in the case of large, complex structures which require many sensing sites and are characterized by interactions between members that are difficult to model accurately on a global scale. In recent years, an effort has been underway, notably in the area of vibration control, to develop *decentralized* control techniques which distribute the control effort throughout the structure, thereby localizing the controller's knowledge and influence. The challenge for the decentralized controller design is to retain global control authority necessary to control the structure as a whole, in spite of the lack of reliance on the global models and the global state information.

In this thesis, we investigate the viability of decentralized control as an alternative to centralized control, as applied to active buckling control of a structural member. In order to compare the performance of the two types of controllers, we conduct qualitative analysis, simulation, and experimentation on a prototype beam. The results indicate that even a very simple, unsophisticated decentralized controller is capable of increasing the load-bearing strength of the beam to the levels comparable to those achieved through the use of centralized control.

Thesis Supervisor: Gerald J. Sussman
Title: Matsushita Professor of Electrical Engineering

Acknowledgments

Many thanks go to my thesis advisors and the leaders of Project MAC, Gerry Sussman and Hal Abelson, for their encouragement, advice, and support over the years.

Andy Berlin, an alumni of Project MAC, initiated the work on active buckling control for the purpose of increasing the load-bearing strength of structural members. I was lucky to be able to gain from his experience first hand, as well as to inherit his experimental setup. Andy is now at Xerox PARC, where this project was started, under his supervision, in the summer of 1995. I am grateful to Andy for his continual help and support that goes above and beyond the scope of this project.

Thanks to all the other people at Xerox PARC who helped me at the initial stages of this project and who made my summer in Palo Alto both educational and enjoyable. Particular thanks to Feng Zhao, Bernardo Huberman, and Tad Hogg for many heated discussions about intelligent structures, distributed control, and beam dynamics. Thanks also to Gregor Kiczales for taking me in as a member of his group, as well as for teaching me how to skate down steps. Next time, I will bring a helmet, and then we can do some real damage!

Likewise, my friends and colleagues at MIT gave me the valuable help and support that helped to pull me through. Special thanks to Elmer Hung, for his tremendous help with every aspect of this project, and for always being there. Thanks also to Daniel Coore, for asking questions and helping figure out answers.

Thanks to all the members and friends of Project MAC, both past and present, for being a memorable part of my life for the last five years. Among them are Stephen Adams, Phillip Alvelda, Joe Bank, Peter Beebee, Becky Bisbee, Michael Blair, Brian Carlstrom, Daniel Coore, Alex the Dog, David Espinosa, Amir Farbin, Arthur Gleckler, Philip Greenspun, Chris Hanson, Elmer Hung, Tom Knight, Kleanthes Koniaris, Brian LaMacchia, David LaMacchia, Jim Miller, Radhika Nagpal, Luis Rodriguez, Brian Reistad, Guillermo Rozas, Olin Shivers, Thanos Siapas, Panayotis Skordos, Rajeev Surati, Franklyn Turbak, Jason Wilson, Henry Wu, and Brian Zuzga. Sometimes they call us "the testosterone floor," and sometimes they are right; one thing we definitely do not lack is character. I have found here a bottomless well of entertainment, and many extraordinary people who have become good friends.

This work was supported in part by an AT&T Graduate Research Program for Women (GRPW) fellowship. I would like to thank the people on the GRPW committee for their interest in my work and the financial support. Special thanks to Jack Brassil, my mentor at AT&T Bell Laboratories, for the time he spends coordinating my fellowship, as well as for two wonderful months at Bell Labs.

This work was also supported in part by the Advanced Research Projects Agency of the Department of Defense, under contract number N00014-92-J-4097.

Portions of this work were performed at the Xerox Palo Alto Research Center and were sponsored by the Defense Advanced Research Projects Agency under contract DABT63-95-C-0025. The content of the information does not necessarily reflect the position or the policy of the Government and no official endorsement should be inferred.

Contents

List of Figures

List of Tables

Chapter 1

Introduction

1.1 Background: Active Structural Control

The idea of active structural control is a rather recent one. Traditionally, civil engineering structures, such as buildings, columns, and bridges, have been built as *passive* structures that rely on their mass and stiffness to resist outside forces and environmental effects. For example, bridges built today are designed with a large safety margin to support dynamically varying loads and vibrations, such as those caused by trains, cars, people, earthquakes, and extreme weather conditions. The desired high levels of safety and reliability of modern structures are attained by resting them on strong foundations, and by using rigid materials to ensure structural stability.

In the last 20 or 30 years, however, research has been underway to develop structures with some degree of adaptability and dynamic responsiveness. Such structures are able to dynamically alter their behavior in order to adapt to their changing environment. For example, with the advent of new materials and new construction methods, buildings are becoming taller, longer, and more flexible, leading to undesirable vibrational levels under large environmental stresses. To counteract this effect, people have proposed constructing "dynamic intelligent buildings" capable of damping out excessive vibrations during critical events, such as earthquakes. Taking the idea of dynamic structures even further, one can imagine buildings being able to change form, shape, and configuration in order to make themselves adaptable to various external forces and functional usages.[1]

As Berlin points out in [7], one can see the appeal of dynamic, or intelligent, structures by comparing man-made structures of today to structures that occur in nature. While our buildings are massive and solid, the structures built by nature (i.e., animals) "contain many flexible joints, bend fairly easily, and are not even secured by foundations. Yet these naturally occurring structures manage to stand up, support loads, and move around with grace and precision"[7, p. 9]. Animals achieve this kind of structural stability by virtue of their ability to actively modify their dynamic behavior. By supplying buildings and bridges with some of the same capabilities, we

[1] See [33] for a multitude of specific examples of intelligent structures, both proposed and built, as well as for a general treatment of active structural control.

hope to some day create man-made structures that behave more like the structures occurring in nature.

The notion of *active control* goes hand-in-hand with the idea of intelligent structures. An actively controlled system incorporates sensing, computing, and actuating elements as part of the structure. During the system's operation, the dynamical state of the structure and/or its environment is continuously evaluated using sensors located throughout the structure; subsequently, the control action is calculated based on the state information so as to alter the structure's behavior in some desired way, and the corresponding control forces are exerted by the actuators, also situated throughout the structure.

The basic concepts of active control are not new; the theoretical basis for active control is rooted in modern control theory (see, for example, references [23] and [19]), which has been with us for many decades. However, application of active control to civil engineering structures presents some interesting new challenges ([33]). One difficulty is that the traditional control techniques rely on global modeling of the systems to be controlled, but obtaining global models of large, irregularly shaped, complex structures may prove difficult if not impossible. Below, we argue that this calls for the development of decentralized control approaches which do not rely on the accuracy of the global models.

1.1.1 Active Control of a Buckling Beam

The particular example of an actively controlled system that is central to this thesis consists of a very simple structural element—a beam (or column)—put under a compressive load. The single most important factor that limits the load-bearing strength of such a beam is the phenomenon called *buckling*. Below a certain critical load, a straight beam is in a state of stable equilibrium: if the beam is perturbed, it will return to the undeflected position once the disturbing force is removed. Above the critical load, the column becomes unstable and fails by bending and deflecting laterally (see figure 1-1).

To increase the load-bearing capacity of a structural element, Berlin in his 1994 Ph.D. thesis, [7], proposed and built a prototype of a system in which buckling of a column is prevented through the use of active control. Intuitively, buckling control is performed by pushing the beam back and forth in the direction of its equilibrium position, thereby preventing its collapse.

To demonstrate the feasibility of the approach, Berlin constructed a prototype actively controlled column, depicted schematically in figure 1-2 (see also figures 2-1–2-3 of chapter 2). The foot-long prototype column is a composite made of steel and piezo-ceramic materials. Arrays of strain sensors located along both sides of the column measure the dynamic state of the structure; similar arrays of piezo-ceramic actuators supply the control forces necessary to counteract buckling. Sensor measurements are supplied to a digital computer, which determines the desired control actions and sends the corresponding control signals to the actuators. The controller works essentially by estimating, given all of the latest sensor information, the current shape of the beam, and computing the control forces that would push the beam in

Figure 1-1: Buckling phenomenon in a real, full-scale structure. A 30-foot tall support beam buckled after being hit by a truck in a May 2, 1996 accident on Interstate 93 in Boston, Massachusetts ([8]). The steel beams are used to support the elevated section of the highway at the point where it crosses the Charles River.

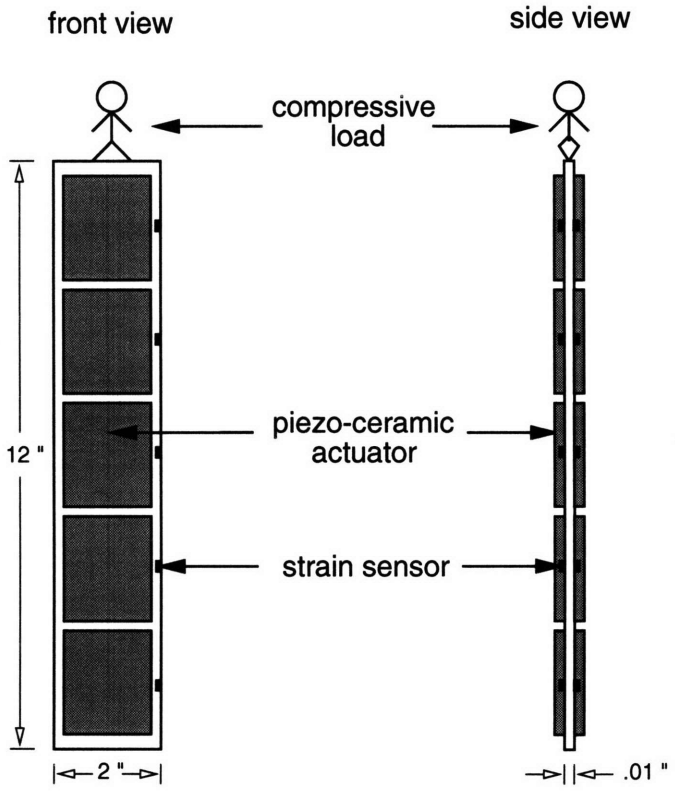

Figure 1-2: Front and side views of Berlin's prototype actively controlled column subjected to a compressive load. The column is of length 12 inches, width 2 inches, and thickness 0.01 inches. Arrays of 5 strain sensors and 5 piezo-ceramic actuators are mounted on each side of the column. Sensor measurements are supplied to a digital computer (not shown), which calculates control signals to be sent to the actuators.

the direction of its undeflected position.

In his experiments, Berlin demonstrated an increase in the load-bearing strength of the prototype beam by a factor of 5.6. This result is very encouraging. Active control of buckling promises to enable us to create structures that are both stronger and lighter than the passive structures of today; taking this notion to an extreme suggests the possibility of building portable structures (e.g., portable bridges). Berlin suggests a variety of possible other applications in [7, chapter 8]; they range from prevention of metal fatigue in ships suffering from wave-induced whipping[2], to building entire cities on top of existing cities by making use of tall actively stabilized columns, an idea originally suggested by Zuk in [39].

[2]This is a phenomenon in which compressive members supporting the hulls of large ships buckle in heavy sea conditions due to wave action pounding on the hull. While the duration of the offensive forces is usually too short to cause immediate failure, repeated whipping causes eventual metal fatigue ([7, p. 98]).

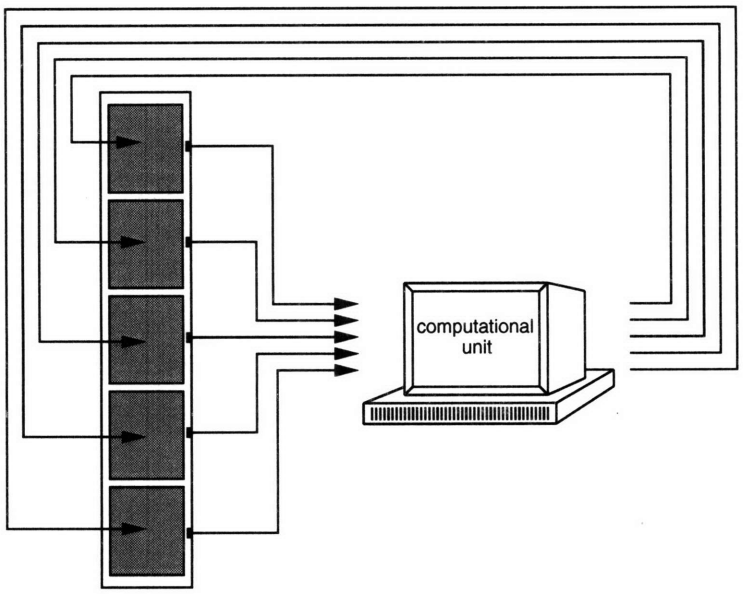

Figure 1-3: A system under centralized control. One computational unit collects all of the sensor information and directs control signals to all of the actuators.

1.1.2 Control Approaches

The type of controller Berlin uses to stabilize his beam is what we call a *global*, or *centralized*, controller. The name refers to the control strategy's utilization of a global model of the system, as well as global state information, to calculate control actions. Figure 1-3 contains a pictorial representation of a system under global control. All of the sensor information is directed to one centralized computational unit, which in turn sends control signals to all of the actuators. The computation of control forces is performed using knowledge about the dynamical behavior of the system as a whole, as well as the sensor information describing the state of the entire system.

Modern control theory is essentially the theory of centralized control: all traditional control techniques assume both the existence of a global model for the system to be controlled, and the availability of global state information. These requirements make it difficult, in general, to apply traditional control techniques to active structural control, for two reasons. First, civil engineering structures tend to be too complex to allow for accurate modeling on a global scale. Secondly, the size and complexity of most real structures requires a great number of sensing sites, which makes it practically impossible to collect all state information in a single place (i.e., the global computational unit) and process it in a reasonable amount of time.

As an example, let us turn again to buckling control. As mentioned above, Berlin was able to prevent buckling of his prototype beam by using centralized control techniques. This was possible because, as we shall see in chapter 3, the global system dynamics of a simple structural element such as a beam can be modeled analytically; this immediately provides us with a global model to use as the basis for centralized control. In addition, the number of sensors and actuators required to control buckling

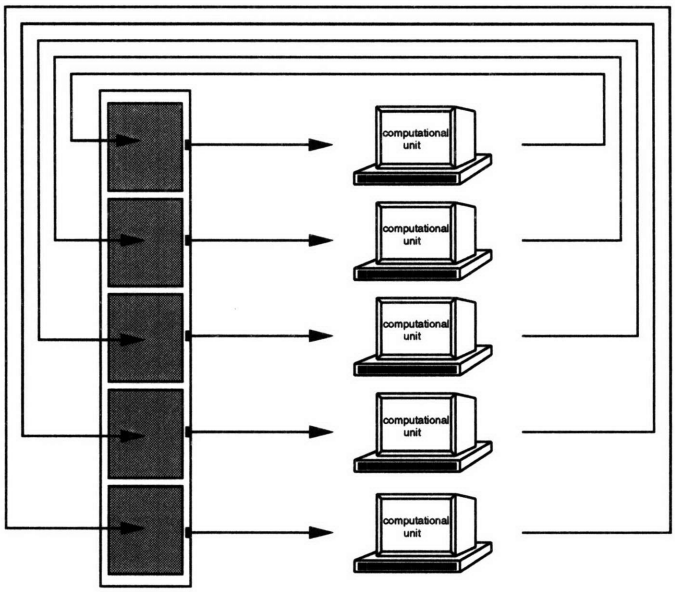

Figure 1-4: A system under decentralized control. The controller employs several computational units, each of which is responsible for controlling a small local region of the structure. In this example, a computational unit is provided for each sensor/actuator pair; the controller is truly *local.*

of a single beam is not prohibitively large; thus, all of the state information needed for determination of control actions can be collected and processed quickly and efficiently.

On the other hand, consider applying full-scale buckling control to a complex structure such as a bridge, a ship, or an airplane—a massive structure composed of many (possibly heterogeneous) structural members. Interactions between the individual members composing such a structure are difficult to model accurately on a global scale. Furthermore, even if we could come up with a global model of such a structure, practical implementation of active control would require a very large number of sensors. A single computational unit would simply not be able to interpret all of the state information quickly enough to be able to respond to it.

The above example demonstrates the need to develop control strategies that rely on neither the global models nor the global state information. We put such control strategies under the general label of *decentralized* control. As we envision them, decentralized controllers employ a multitude of computational units, each of which is responsible for controlling only a small *local region* of the entire structure. More precisely, each computational unit processes state information provided by the sensors located in its region, and generates control signals to the actuators in the region. Thus, there is no reliance on global state information in the determination of control actions. Furthermore, control signals are generated based purely on the local behavior of the system; no global models are utilized. Figure 1-4 demonstrates the decentralized approach, which should be contrasted with the centralized method of figure 1-3.

The main drawback of the decentralized control approach is that because of the lack of global information available in the computation of control actions, the overall control strategy implemented by a decentralized controller may not be globally opti-

mal. The challenge faced by the control designer is to come up with a decentralized control strategy that retains global control authority, and thus yields effective global behavior.

In this thesis, we compare the centralized and decentralized control approaches for the specific case of a buckling beam. To prevent the beam from buckling, a centralized controller continuously estimates, given the global sensor information, the shape of the entire beam, and tries to push the beam in the direction of its undeflected position. Under local control, the beam is treated instead as a collection of small segments; for each segment, the controller determines, and tries to reduce, the local curvature. It is clear that both controllers, if successful, have the effect of keeping the beam close to the desired (straight) position, although the strategies employed are very different.

1.2 Related Work

Before diving into the details of the work performed in this thesis, let us briefly summarize prior work related to buckling control, as well as to centralized and decentralized control methods.

1.2.1 Buckling Control

A good summary of work related to active control of buckling conducted prior to Berlin's experiments is given in [7, chapter 2]. According to Berlin, "until recently, little attention has been given to the possibility of controlling buckling for the purpose of increasing the load-bearing strength of a structure" [7, p. 15]. Berlin was the first to demonstrate experimentally that the load-bearing capabilities of compressive members could be increased through active buckling control.

Berlin's experimental work was not limited to control of the prototype steel column described above. To test the feasibility of active buckling control, Berlin first constructed a prototype column in which the control forces are applied by tendons at the midpoint of the column. A single pair of strain gauges was used to measure the curvature of the column at its midpoint. Through active control of buckling, the load-bearing strength of this simple prototype beam was shown to increase by a factor of 2. To demonstrate the possibility of incorporating more than one actively stabilized structural element into a structure, Berlin also constructed a railroad-style truss bridge with two compressive members controlled through the use of piezo-ceramic actuators. In addition to tendons and piezo-ceramic actuators, Berlin proposes a variety of other actuation strategies in [7, chapter 7], and suggests some applications in which these different strategies might prove useful.

In all of his experiments, Berlin employed a centralized approach to buckling control. In particular, his prototype steel column was controlled via "modal" control methods, introduced below. To our knowledge, no decentralized approach to active buckling control has previously been attempted.

1.2.2 Vibration Control

While control of buckling is a direction rather new in active structural control, there has been significant effort devoted to the study of vibration control. One of the main applications is active vibration suppression in flexible satellites and other large spacecraft ([9], [31], [1], [29], [2], [5]); others include active damping of tall buildings and active optics ([33]).

In some ways, active vibration control is similar to active control of buckling. Both types of controllers aim to minimize the motion of a structure away from its equilibrium position. However, in the case of vibrating structures, the equilibrium is stable; the job of the controller is to reduce the amplitude of oscillations. Structures undergoing buckling, on the other hand, are inherently unstable and will collapse if control is removed. In buckling controllers, then, there is much less tolerance for runtime failures and inaccuracies in the system model.

Another important point is that buckling control depends inherently on the actuator strength—the amount of force an actuator is capable of exerting. The greater the actuator strength, the more weight can be supported by an actively controlled structure. Limitations on actuator forces yield nonlinearities in the control strategy. Buckling controllers have to take these nonlinearities into account; we shall see the implications of this for buckling controller design in chapter 2.

Despite these key differences, many of the techniques developed in vibration control are applicable to buckling control. These include both centralized and decentralized approaches, which we summarize below.

1.2.3 Centralized Control Strategies

The global approach that, over the last several years, has become the strategy of choice for control of large structures is *independent modal space control* (IMSC), introduced by Meirovitch ([22], [5], [33]). This method decouples the high-order dynamical system into a set of independent second-order systems, expressed in terms of "modal" coordinates. The control design is then carried out for each second-order system independently. The resultant "modal forces" have to be transformed from the modal space to the actual control forces to be applied. We will be looking at IMSC much more closely throughout this thesis; from now on, we will refer to it simply as *modal* control.

Other common methods of centralized control, including pole allocation, linear optimal control, and nonlinear on-off control, are referred to as the "coupled" approaches. These techniques were originally designed for systems in which the number of sensors and actuators is small relative to the plant dimension, and are not well-suited for control of large structures with multiple sensing and actuation sites. In [22], Meirovitch et al. show that IMSC holds many advantages over the coupled methods, which are more difficult to design and implement and require greater computational effort.

1.2.4 Decentralized Control Strategies

Most of the work on decentralized control has been done in the area of vibration control of large flexible space structures. A typical strategy is to decompose the system into a number of local subsystems, and to design individual controllers for each of the subsystems; any interactions between the subsystems are ignored. Examples of this approach can be found in [29], [38], [6], and [27]. In addition, there has been some theoretical work on establishing the robustness and stability characteristics of decentralized control methods ([12], [37], [36], [32], [16]). Many of the results pertaining to decentralized control techniques are summarized by Sandell et al. in [30].

The decentralized control techniques have been observed to work best for systems that can be naturally subdivided into lightly coupled subsystems. Strongly coupled structures, on the other hand, suffer from the lack of global control authority inherent in decentralized methods. In such systems, *multilevel* controllers have been used as an alternative to purely decentralized designs ([30]). In this approach, control is performed on both local and global levels. For example, Pitman and Ahmadian in [27] describe a multilevel design in which the local controllers are designed for performance, and the global controller is designed to minimize the coupling between the local subsystems. One disadvantage of this approach, however, is that it requires that the central controller have access to all the state information at the local level. More recently, Hall et al. ([13], [15]) presented a *hierarchic* control architecture in which control is achieved by a two-level combination of a centralized controller and a set of distributed residual controllers. The global controller handles the longer wavelength motions of the structure which cannot be effectively influenced by the local controllers, and only requires access to an aggregate of the local state information.

1.3 The Focus of This Work and New Results

As a first step toward exploring decentralized approaches to active control of buckling, this thesis investigates the viability of decentralized control as an alternative to centralized control for the specific case of a buckling beam. Specifically, we compare two particular controllers, one centralized, another decentralized. The global approach used in our comparison is a modal (i.e., IMSC) controller. Our decentralized controller is what we call a purely *local* controller: the control system is decomposed into as many subsystems as there are sensor/actuator pairs[3], and each actuator receives control signals based only on the readings of the associated sensor (see figure 1-4).

In order to compare the performance of the modal and local controllers, we conduct qualitative analysis, simulation, and experimentation on a prototype beam. The results indicate that our local controller is capable of increasing the load-bearing strength of the beam to the levels comparable to those achieved through the use of

[3]In our system, there happen to be as many sensors as there are actuators; each sensor/actuator pair is collocated at some position along the beam. In general, the number of sensors and actuators may be unequal, in which case the definition of a local controller could be modified to include several sensors or actuators for each local subsystem.

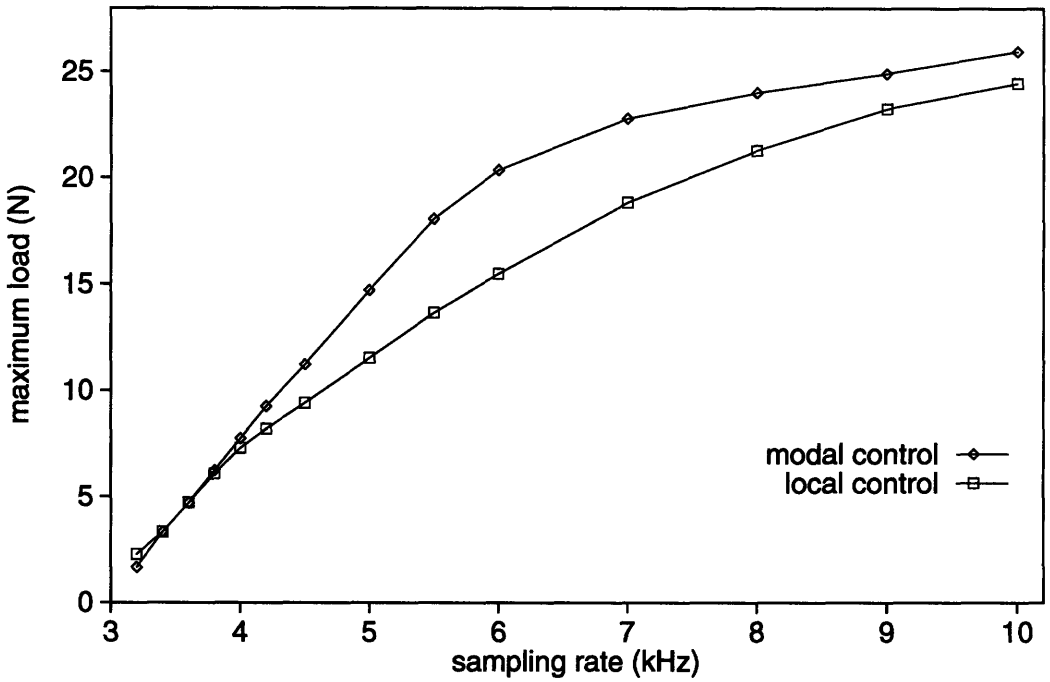

Figure 1-5: Simulation results comparing the performance of the modal and local controllers. The maximum load the beam is able to support (in Newtons) is plotted against the sampling rate of the controller (in kHz). The buckling load (i.e., the maximum load supported by an uncontrolled beam) for this beam is approximately 1.5 Newtons.

modal control. This is demonstrated in figure 1-5, which shows simulation results comparing the two control laws. One of the main factors influencing the amount of weight the actively controlled beam can support is the frequency with which the controller samples and responds to the state of the system; figure 1-5 shows the maximum load supported by the beam with respect to this sampling frequency. We can see from the plot that, although for the most part, the local control curve stays below the modal control curve, the local controller does not do much worse than the modal one. We will have much more to say about this particular plot, as well as the general limitations and advantages of each of our two controllers, in chapters 3 and 4.

The prototype beam employed in the experimental portion of this work is the beam built and used by Berlin in [7]. The results of the physical experiments indicate that the beam under modal and local control is able to support loads of 19.4 and 16.8 Newtons, respectively. With the maximum load supported by an uncontrolled beam measured at 5.3 Newtons, this translates into factors of 3.7 and 3.2 improvement of the load-bearing strength of the beam achieved through active control.[4] As in simulation, here again we observe a rather modest difference in performance of the two controllers.

These results indicate that the decentralized approach holds a promise for active control of buckling.

[4]The sampling rate used by the controllers on the actual beam is 3.8 kHz.

1.4 Overview

In the rest of this document, we describe the work leading to the main results outlined above, and provide a more detailed discussion of the results.

Chapter 2 supplies the general background for the rest of the thesis. We describe in more detail the experimental setup and the control system. We also motivate the choices made in controller design and implementation given the system at hand.

The main bulk of the thesis is contained in chapters 3–5. Chapter 3 reviews the dynamics of an axially-loaded beam under active control, and presents qualitative analysis comparing the modal and local controllers. In chapter 4, we describe computer simulations performed in order to evaluate the relative performance of the two control strategies, and discuss the results of these simulations. The experimental tests and results are presented in chapter 5.

Chapter 6 summarizes the main results obtained in this thesis, and suggests directions for possible future work.

Chapter 2

Setup

The purpose of this chapter is to provide the necessary background for the rest of the thesis. In particular, we describe the experimental setup which is taken as the basis for this work, and take a look at the control system and its components.

2.1 Experimental Apparatus

As mentioned in chapter 1, the experimental apparatus used in this thesis was originally built by Berlin as part of the work described in his Ph.D. dissertation, [7]. Our experiments use all of the same hardware, which we briefly describe below; for more details, the reader is referred to [7, chapter4].

The apparatus used in the buckling control experiments is pictured in figure 2-1.[1] The beam is held in a vertical position with the help of an assembly made of steel, planted on a wooden base. Wires run from the strain gauges on the beam to a circuit board located in front of the beam assembly, where the strain readings are amplified and passed on to the control computer. The equipment behind and to the left of the beam assembly consists of high voltage power supplies and amplifiers that accept control signals from the computer and use the amplified signals to drive the actuators.

In what follows, we describe in more detail the beam assembly, and the principles behind sensing and actuation employed in the system.

2.1.1 Beam Assembly

The column in our experiment is designed to approximate a *simply supported* beam, meaning that the lateral displacement is zero at the two ends of the beam, but the ends are free to rotate. This condition is enforced by pinning the bottom end of the beam, and allowing the top end to move freely in the axial (vertical) direction. As shown in figures 2-2 and 2-3, two hinges are used to connect the ends of the beam to the rest of the beam assembly. The hinges hold the beam in a vertical position when

[1] The photographs of the experimental apparatus presented in figures 2-1–2-4 were taken by Philip Greenspun. Figures 2-1–2-3 originally appeared in Berlin's dissertation, [7]. They are reprinted here with permission of Andy Berlin.

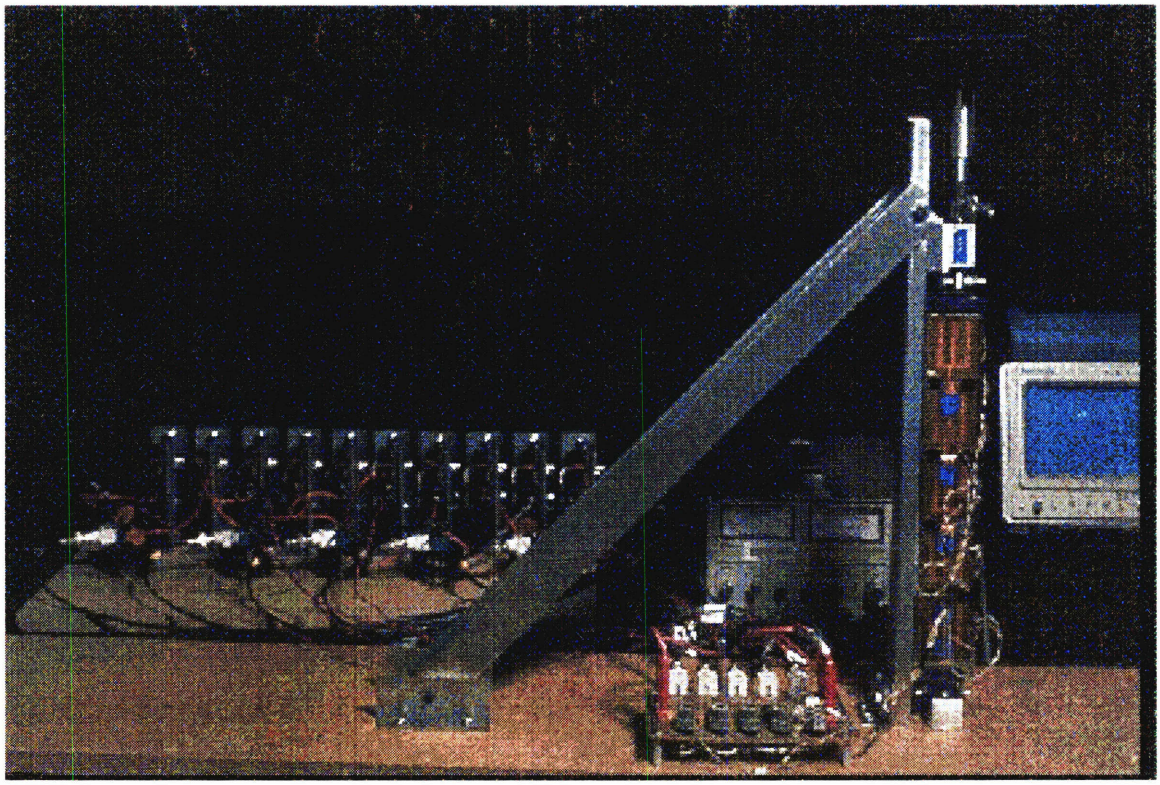

Figure 2-1: Experimental apparatus, consisting of the beam assembly, the strain gauge amplifiers, and the high voltage power supplies and amplifiers which drive the actuators. Both sets of amplifiers are connected to the control computer, not shown here.

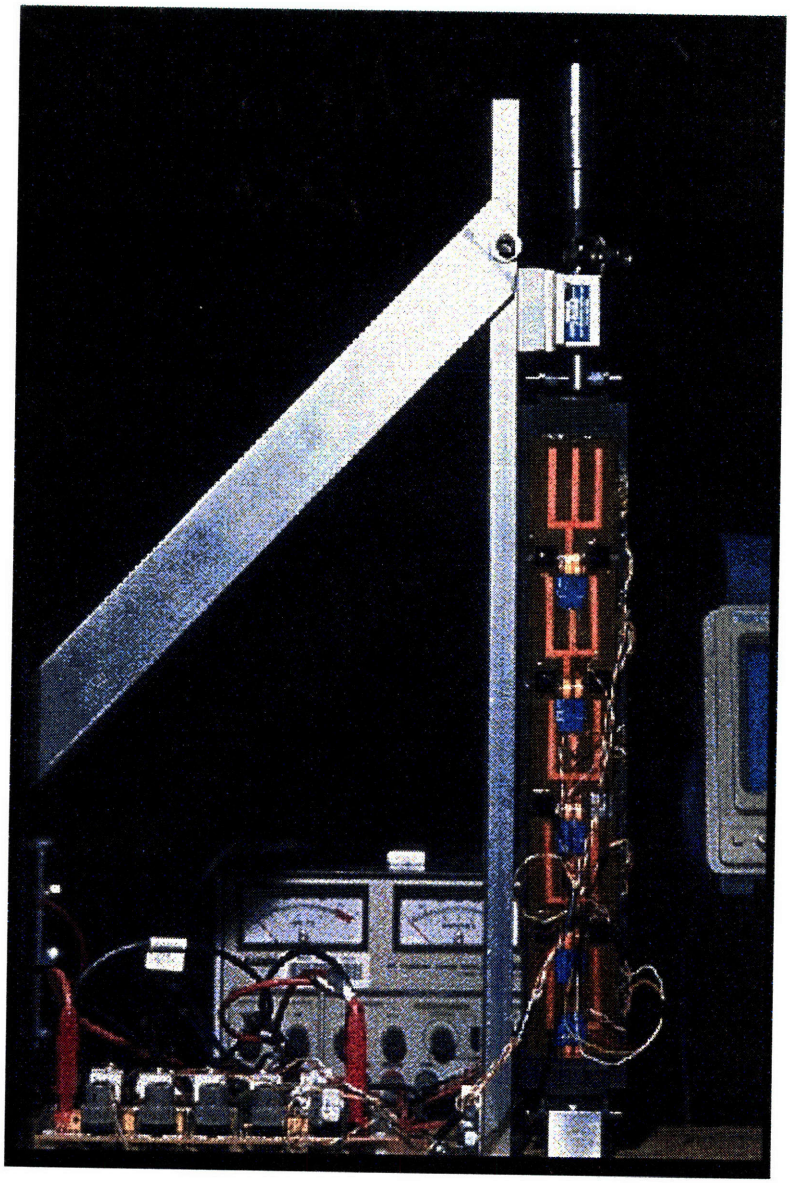

Figure 2-2: Front view of the prototype beam, subject to simply supported end conditions. The beam is connected to the assembly via a pair of hinges. A compressive load can be applied to the beam via a steel rod sliding vertically through a ball bearing. An aluminum clamp is placed on the rod above the ball bearing to prevent complete collapse of the column during buckling.

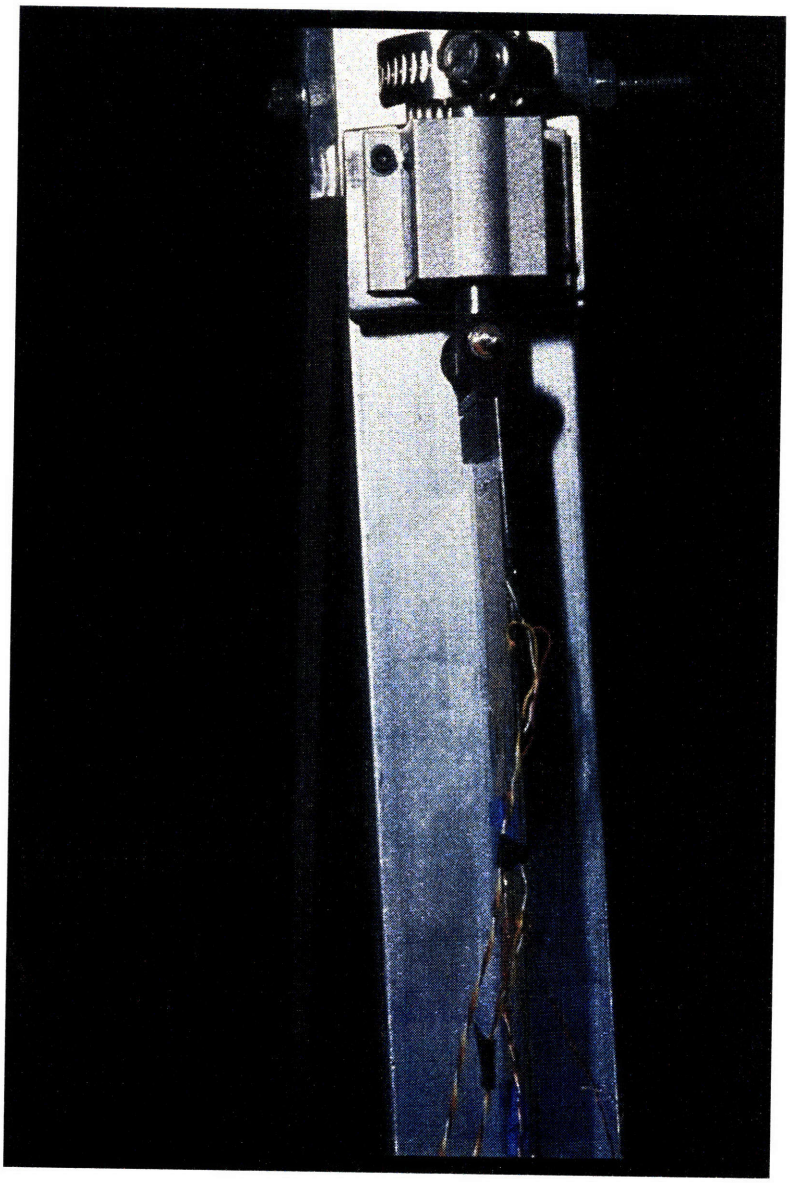

Figure 2-3: Side view of the prototype beam.

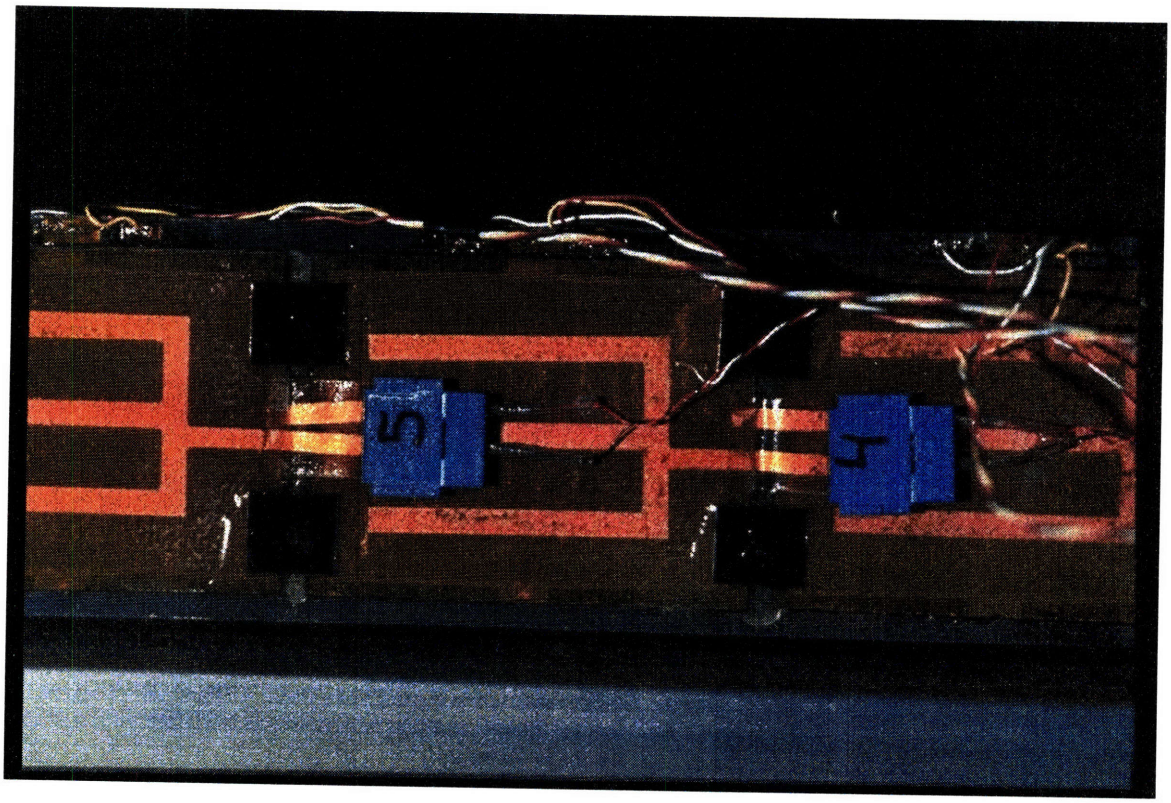

Figure 2-4: A closeup of the beam (view from the top). The column is covered with piezo-ceramic actuators. The gaps between the adjacent actuators are bridged by small 0.01 inch thick steel stiffeners.

no axial load is present, but allow it to bend under the influence of a compressive load. Lateral movement of the top and bottom of the column is prevented by connecting the hinges to two vertically aligned pin joints, which are held stationary in the horizontal direction. A compressive load is applied to the beam by placing it on top of a steel rod, which is allowed to slide up and down through a ball bearing (see figure 2-2). When the uncontrolled column is subjected to a load in excess of the critical load, the axial force thus applied pushes the rod down, resulting in the lateral bending of the column. In order to prevent the column from collapsing when buckling occurs, an aluminum clamp is placed on the rod slightly above the place where it passes through the ball bearing. The clamp acts to constrain the downward movement of the rod, thus guaranteeing the safety of the column.

The steel column has dimensions 12 inches by 2 inches by 0.01 inches (see figure 1-2). A closeup of the beam is shown in figure 2-4. Arrays of 5 strain gauges and 5 piezo-ceramic actuators are located on each side of the column. Each of the actuators is approximately 2.2 inches long and 1.75 inches wide. Thus, the actuators do not cover the entire length of the column; as can be seen from figure 2-4, there are small gaps (approximately 0.1 inches wide) between adjacent actuators. To prevent local bending of the column in these gaps, small 0.01 inch thick steel stiffeners are mounted between adjacent actuators.

2.1.2 Sensing

As we saw in figure 1-2, sensing in the system is provided by a total of 10 strain gauges. Each pair of strain gauges, located on the two sides of the beam, is used to measure the strain at one of the 5 points along the length of the beam. Two sensors rather than one are used at each point to provide for more accurate and reliable measurement: the value supplied to the control computer is actually the difference in strains measured by the two sensors.

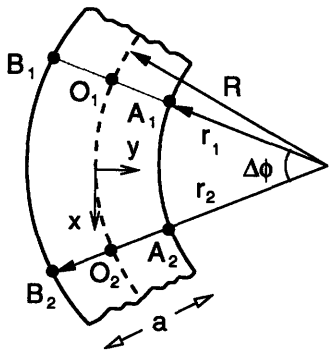

Figure 2-5: Side view of a deformed beam segment for a beam of thickness a.

To better understand the significance of the measurements being taken by the sensors, consider a small segment of a deformed beam displayed in figure 2-5. The coordinate system associated with the beam is shown in the figure: x indicates the location along the length of the beam, while y represents the deflection of the center of the beam (along the column's thickness) away from the straight position. Let a be the thickness of the beam; then we observe that each of the two sensors is located a distance $\frac{a}{2}$ away from the center of the beam.

We assume in figure 2-5 that when the beam segment is deformed, the originally straight longitudinal lines turn into arcs of circles (see [11, pp. 418–21]). The figure shows the radii of curvature R, r_1, and r_2 of the arcs corresponding to the center, the right side, and the left side of the beam, respectively. The angle $\Delta\phi$ spans the arc segments O_1O_2, A_1A_2, and B_1B_2 of interest. Notice that, in the figure, the arcs on the left side of the beam become longer, while those on the right

side become shorter as a result of the deformation. We assume that the length of the centre arc O_1O_2 stays equal to the straight line distance between the points O_1 and O_2 in the undeformed beam (see [11, pp. 424]).

Strain can be defined as the fractional change in the original length of a material; thus, the center of the column experiences zero strain, while the strain at the right end is given by

$$\epsilon_{right} = \frac{r_1\Delta\phi - R\Delta\phi}{R\Delta\phi} = \frac{-\frac{a}{2}\Delta\phi}{R\Delta\phi} = -\frac{a}{2}\frac{1}{R}$$

and similarly,

$$\epsilon_{left} = \frac{r_2\Delta\phi - R\Delta\phi}{R\Delta\phi} = \frac{a}{2}\frac{1}{R}$$

The difference in strain measured by the right and left sensors is then given by $-a\frac{1}{R}$, where $\frac{1}{R}$ represents the curvature of the beam at the location of the sensors. For small deformations, curvature can be approximated by the second derivative of displacement (see [11, p. 514]), yielding the following expression for the difference in strain:

$$s(x) = -a\frac{d^2y}{dx^2} \tag{2.1}$$

We will make use of expression (2.1) in chapters 3 and 4, when discussing the control strategies used to prevent the beam from buckling.

2.1.3 Actuation

The actuators used in the experimental system are made of piezo-ceramic. When an electric field is applied to a piezo-ceramic material, it induces stress in the piezo-ceramic, causing it to either grow or shrink, depending on the polarity of the field. With a piezo-ceramic actuator mounted on the side of a column, application of an electric field results in forces being exerted on the beam by the actuators in an attempt to relieve the stress induced in the piezo-ceramic.

To be more specific, the actuation proceeds as follows. Given some control voltage V, the corresponding electric fields of equal magnitude but opposite polarities are applied to the actuators on the two sides of the beam, causing one of them to grow and the other to shrink. This produces a longitudinal control force F applied at the endpoints of the actuators; F is tensile on one side of the beam, and compressive on the other (see figure 2-6a). The overall effect of the induced electric field is a pair of bending moments Fa (neglecting the actuator thickness), applied at the endpoints of the actuators; this is demonstrated pictorially in figure 2-6b.

As mentioned in chapter 1, an important parameter in active buckling control systems is the actuator strength—that is, the amount of force an actuator is capable

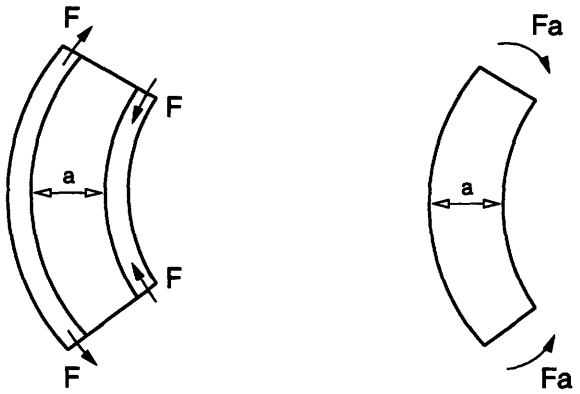

Figure 2-6: Actuation of a piezo-ceramic material mounted on the two sides of a beam. In (a), the actuator on the left side of the beam is growing, thus applying a tensile longitudinal force F to the left side of the beam segment, while the actuator on the right side of the beam is shrinking, yielding a compressive force F at the right end of the segment. The bending moments Fa produced by these longitudinal forces are shown in (b).

of exerting. The piezo-ceramic actuators used in our experimental system can be subjected to voltages as high as 200 Volts; this corresponds to the maximum applied bending moments of roughly 0.14 Newton-meters.

Further details regarding the principles of piezo-ceramic actuation can be found in [7, pp. 36–40]. For example, [7] explains the relationship between the applied voltage V and the resultant actuator forces F, and discusses some nonlinear properties of the piezo-ceramics.

2.2 Control System

The control system used in the active buckling control experiment is an example of a *closed-loop*, or *feedback* system. Such a control system continuously compares the actual state of the structure (the feedback signal) with the desired state, and uses the difference, or *error*, as a means of control. The aim of the controller is to reduce the error and bring the system to the desired state. In our case, the goal is to keep the beam in (or close to) its undeflected position, and the size of the error is measured by the magnitude of the beam's deflection away from that position. As we saw earlier in this chapter, the state of the structure is determined with the help of strain sensors, and the desired control forces are exerted by piezo-ceramic actuators. In addition to the forces induced by the actuators, the dynamics of the beam may be affected by external excitations (e.g., banging of a fist on the table).

A block diagram of the control system is depicted in figure 2-7. Here, the *plant* is the uncontrolled system, represented by the transfer function $G_2(s)$. Its output $X(s)$ represents the state of the system. The actual state $X(s)$ is fed back to a subtractor,

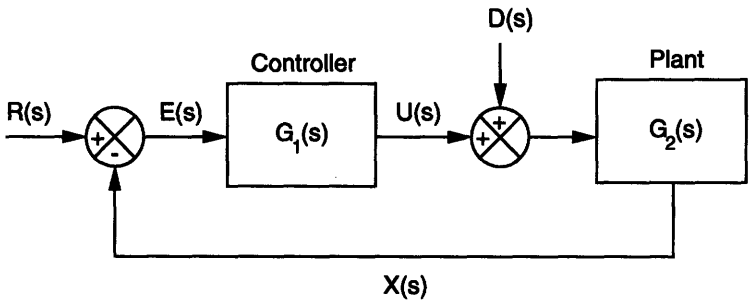

Figure 2-7: Block diagram of an active control system. The actual state of the plant $X(s)$ is subtracted from the desired state $R(s)$ to produce the error $E(s)$. The controller with transfer function $G_1(s)$ turns this error into a control action $U(s)$, which is used to influence the dynamics of the plant. $D(s)$ represents the external excitations affecting the behavior of the system, and $G_2(s)$ is the transfer function describing the dynamics of the plant.

which compares it to the desired state, $R(s)$, and produces the error $E(s)$. This error is acted upon by the controller with transfer function $G_1(s)$ to produce the control action $U(s)$, which, along with the external disturbance to the system $D(s)$, forms the input to the plant.

Note that, in this chapter, we are being purposefully vague about what we mean by the "state" of the system. In general, there is more than one way to represent the system's state. For example, state in our system can be represented by a vector of 5 strain values measured by the sensors, plus their derivatives with respect to time. Another possibility is to base the control on the beam's deflection from the vertical (along with the derivative of the deflection); in this case, the sensor measurements have to be converted, via double integration (see equation (2.1)), to a measure of displacement. Thus, the state of the system is not necessarily measured by the sensors directly.

When we introduce modal and local control in chapter 3, we shall see that the two controllers employ two different representations of state. By not committing ourselves to any one state representation at the moment, we can talk about the high level issues in control system design and implementation regardless of the specific control approaches being used.

2.2.1 PD Control

Although the modal and local controllers employ different state representations, the control law transfer function $G_1(s)$ used by the two controllers in our system is the same. This transfer function implements *proportional* plus *derivative* control, or simply PD control. The main reason for choosing PD control from among a variety of control strategies available to a control designer is the simplicity of analysis and implementation that PD control provides. Berlin used a variant of PD control (what he termed "PIDV control") in his system ([7, pp. 54–9]) as well.

As indicated by its name, the action of a PD control law is composed of the response to the state of the system as well as its derivative. That is, the equation of

a PD controller is given by

$$u(t) = Pe(t) + D\frac{de(t)}{dt} \tag{2.2}$$

where $e(t)$ and $u(t)$ are the input error signal and the controller output, respectively. In the frequency domain, the transfer function of a PD controller is thus

$$G_1(s) = \frac{U(s)}{E(s)} = P + Ds$$

The constants P and D are termed the proportional and derivative *gains*, respectively. The gains are chosen by the control designer such that the system exhibits the desired response for various kinds of inputs. We will have more to say about the process of gain selection shortly.

Intuitively, proportional control, in which the control action is proportional to the error, makes sense: if the error is large, a large corrective action is applied; if the error is small, a small corrective action is applied. Thus, proportional control tends to stabilize the system. Derivative control action, when added to a proportional controller, provides a means of obtaining a controller with high sensitivity. Derivative control responds to the rate of change of the actuating error and can produce a significant correction before the magnitude of the actuating error becomes too large. It thus helps prevent overshoot by anticipating the actuating error and initiating an early corrective action. One should note, however, that while high sensitivity of the derivative control gives the controller an anticipatory character, it also amplifies the high frequency noise present in the system. A more detailed discussion of PD control can be found in any control theory text, such as [23] or [19].

2.2.2 Determining Optimal Control Gains

It remains to specify the gains to be used in the PD control law. In modern control design,[2] control parameters are typically determined via pole placement or linear optimal control (see [23, chapter 10], [33]). The idea behind these methods is to identify a set of control gains that minimize some prespecified *performance index*. The performance index provides a measure of how much the system's actual performance deviates from the ideal performance. For example, linear optimal controllers often employ quadratic performance indexes, which are quadratic functions of both the error signal and the energy required for control action, integrated over some period of time. Calculating the control parameters which correspond to the minimal performance index of this type requires solving the algebraic Riccati equation; several efficient solution methods are documented in the literature ([33]).

[2]Modern control theory utilizes state-space methods, and is applicable to complex multiple-input, multiple-output systems. It was developed as an alternative to conventional control techniques which operate in frequency domain and are only applicable to single-input, single-output systems ([23]).

Like most control design techniques, modern control state-space methods are only applicable to linear time-invariant systems and yield linear control laws (hence the name "linear optimal control," for example). While all physical systems are nonlinear to some degree, most of them can be approximated as linear over a limited range of operation, and linear control techniques can still be used.

In buckling control, however, while the plant itself can be approximated by a linear system, the controller turns out to be inherently nonlinear. The difficulty stems from having actuators of limited strength. The actuators at hand may fall short of realizing the control signal $u(t)$ for some time t, in which case the control signal has to be cut off, or *saturated.* Thus, actuator limits introduce nonlinearities in the control law. Because of these nonlinearities, optimal control gains for buckling controllers cannot be calculated via linear control methods directly.

Although all control systems involve actuators of finite strength, in most systems actuator limits are not of major concern. For example, vibration controllers can often be designed to have gains small enough that the desired control forces never exceed the actuator limits, thus avoiding the associated nonlinearities. This may handicap the controller somewhat, since it might not be using all of the available control authority; however, this usually has only a minor effect on the system performance. In buckling control, on the other hand, actuator limits directly affect the amount of weight the beam can support. A controller which is not using all of the control authority available to it will fail at loads smaller than it could have supported were it allowed to utilize the actuators to their fullest. Since the question of the maximum sustainable load is of major importance in this thesis, we cannot ignore the nonlinearities associated with limited actuator strength while calculating the optimal control gains.

Instead of using one of the state-space methods, we thus turn to numerical optimization techniques to compute the control gains. Numerical optimization routines still make use of a performance index, frequently termed the *merit function.* Optimization consists of searching the space of variable controller parameters in order to find a point in the space where the merit function is minimized. The particular optimization technique we use is the *downhill simplex method* by Nelder and Mead, described in [28]. This method is extremely straightforward, and makes almost no special assumptions about the function to be minimized. The algorithm starts with an initial guess at the parameter values. At each step in the algorithm, the dynamics of the beam are observed for some specified period of time, and the merit of the control gains is evaluated using the performance index. The performance index employed is similar to the quadratic performance indexes used by linear optimal controllers: it is a quadratic function of both the deflection of the beam and the velocity with which the beam is moving, integrated over time. The beam's deflection indicates the magnitude of the error signal, while the velocity of the column provides a measure of kinetic energy present in the system. A more detailed description of this merit function, as well as the optimization process itself, is provided in chapter 4.

A major difficulty with this optimization approach is that the minima found by the optimization routine may be local rather than global. We can use some ad hoc techniques to avoid getting trapped in local minima: for example, optimization can be performed several times, starting with different initial values of control gains, and the

best result among all the runs can be chosen. In addition, we can help the optimizer by picking "good" initial parameters by hand. Finally, optimization can be restarted at a point where it claims to have found a minimum; this may allow the routine to climb out of a local valley in which it might have gotten trapped (see [28, p. 410]).

With all these caveats, the optimization process can become rather computationally demanding and time-consuming. On the other hand, it provides a convenient, largely automatic way of obtaining optimal control gains for the system with nonlinear characteristics.

As a final note on optimization approaches, it is worth mentioning that the optimization process described here is similar to the techniques used in *optimalizing control systems* presented by Ogata in [23]. These systems exemplify *adaptive* controllers, which seek to accommodate unpredictable environmental changes affecting the dynamics of a plant. For a plant experiencing large variations in environmental conditions (either within the system itself or external to it), it is usually not possible to design a single control law that would yield satisfactory system performance under all conditions. Thus, adaptive controllers have to continuously measure the dynamic characteristics of the plant and adjust the control parameters so as to compensate for changes in the plant dynamics. In optimalizing control systems, control parameter adjustment is performed based on an optimization routine much like the one described above. As Ogata points out in [23, p. 855], the greatest advantage of this approach is that no restrictions are placed on the plant: it can be nonlinear, time-varying, and so on.

Ultimately, of course, we would like the buckling controllers described in this thesis to be able to adapt to changes in environmental conditions. In the future, the optimization approach presented here may prove useful in the development of techniques for adaptive control of buckling.

Chapter 3

Qualitative Comparison

We are now ready for qualitative analysis of the system described in chapter 2. We start by deriving the dynamics of an axially-loaded beam subject to control forces. We then take a closer look at modal and local controllers, in particular. By the end of the chapter, we gain some insights into the system's behavior under both kinds of control, as well as the relative advantages and disadvantages of the two approaches.

3.1 Beam Dynamics

Consider a simply supported *ideal* beam of length L, width w, and thickness a, shown in figure 3-1. For simplicity, in the analysis of this chapter the beam is assumed to be uniform. The coordinate system associated with the beam is as indicated in figure 3-1. The beam is subjected to an applied axial load W, also shown in the figure.

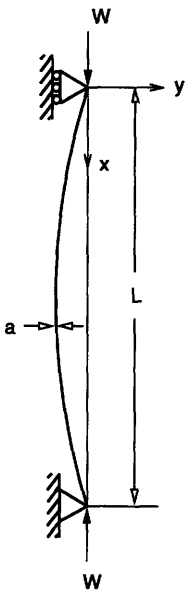

Figure 3-1: A simply supported ideal beam under an axial load, W.

In addition to the beam's physical dimensions, equations below involve the following material properties of the beam: Young's modulus E, beam mass per unit length ρ, and area moment of inertia $I = wa^3/12$.

We assume that the length of the beam L is large compared to its width w and thickness a. When a short column is put under a gradually increasing compressive load, it eventually fails by crushing. When the column is long, however, it will fail by buckling, that is, by bending and deflecting laterally, rather than failing by direct compression, at a load W very much smaller than is required to crush the material.

Typically, the buckling phenomenon is explained by analyzing the stability properties of a loaded beam in *static* equilibrium (see [14], [11], and [34]). It can be shown that if the axial load W is below a certain critical value, termed the *buckling load*, the system is in *stable* equilibrium—that is, if the beam is disturbed, it will return to the straight position once the disturbing force is removed. As W is gradually in-

creased, a condition of *neutral* equilibrium is reached when W is equal to the buckling load; at this load, the beam may theoretically have any small value of deflection, and a small lateral force will produce a deflection which does not disappear when the force is removed. At loads higher than the critical load, the beam is *unstable* and will collapse. The value for the buckling load can be obtained by solving the differential equation governing the deflection of the beam in static equilibrium.

Instead of taking the static approach, however, we study buckling behavior by considering the dynamics of a beam in motion. In practice, a slender column such as the one in figure 3-1 is subject to many perturbations induced by the environment, and is thus never perfectly still. By studying beam dynamics, we will be able to understand and predict the response of the beam to external forces and perturbations, explain the origins of buckling, and come up with ways to prevent the buckling behavior.

Below, we first gain some insight into the natural response of the system to perturbations, by taking a look at free vibration of an unloaded beam. We then discuss how applying an axial load changes the dynamics of the beam and introduces a potential for instability. Finally, we consider the effects of applying control forces aimed to stabilize the beam's vibrations, thereby preventing its collapse.

3.1.1 Free Vibration

Suppose an unloaded beam is initially at rest in its equilibrium position—i.e., the straight position, $y(x)=0$. At time $t=0$, some external force is applied to the beam, causing a deflection away from the original equilibrium. If the external force is then removed, the beam will vibrate; such motion is called *free vibration.*

Because $w \ll L$, we assume that the deflection y of any point on the beam depends only on its location x along the length of the beam and on time t, and not on its position along the width of the beam. The equation of motion of the beam is thus a partial differential equation which describes how the displacement y varies with respect to x and t.

In order to obtain the equation of motion of a vibrating beam, we take a look at the forces and bending moments applied to an infinitesimal segment of the beam (considered as a free body), pictured in figure 3-2. The segment is located at a distance x from the left end of the beam (oriented horizontally for convenience), and is of length dx; the time-varying lateral displacement of the segment is given by y. Applied at the two ends of the segment are the shear forces $V(x,t)$ due to the adjacent segments of the beam, and the bending moments $M(x,t)$ associated with the beam's deflection. If we designate the shear force at the left end of the segment by V, and the bending moment by M, then the corresponding quantities at the right end can be expressed as $V + \frac{\partial V}{\partial x}dx$ and $M + \frac{\partial M}{\partial x}dx$. Finally, the acceleration of a vibrating beam segment is given by $\frac{\partial^2 y}{\partial t^2}$, resulting in an inertial force $\rho\, dx \frac{\partial^2 y}{\partial t^2}$ in the negative y direction.[1]

For our system to be in *dynamic equilibrium*, both forces and moments must be balanced about an arbitrary point on the beam ([35, p. 241]). Applying these

[1] See [11, pp. 158–60] for a more detailed derivation of the equations associated with figure 3-2.

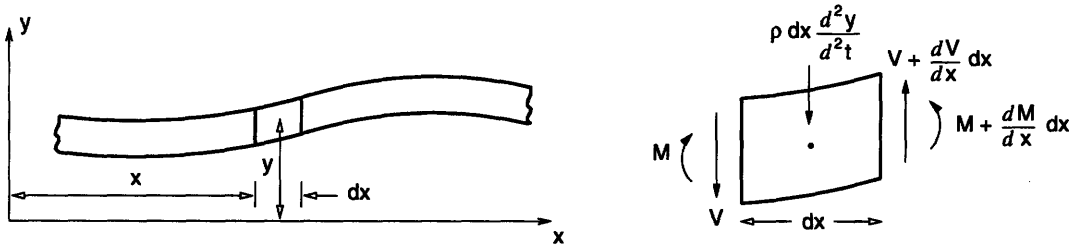

Figure 3-2: Unloaded beam in free vibration. Each differential beam segment is subjected to shear forces $V(x,t)$ due to the adjacent beam segments, and bending moments $M(x,t)$ transmitted by the deflected beam. The inertial force exerted on the segment due to acceleration in the y direction is $\rho\, dx \frac{\partial^2 y}{\partial t^2}$.

equilibrium conditions to the beam segment of figure 3-2, we obtain the following two equations:

$$(V + \frac{\partial V}{\partial x}dx) - V - \rho\, dx \frac{\partial^2 y}{\partial t^2} = 0 \tag{3.1}$$

$$(M + \frac{\partial M}{\partial x}dx) - M + (V + \frac{\partial V}{\partial x}dx)\frac{dx}{2} + V\frac{dx}{2} = 0 \tag{3.2}$$

Simplifying, and discarding the higher order terms in equation (3.2) yields

$$\frac{\partial V}{\partial x} = \rho \frac{\partial^2 y}{\partial t^2} \tag{3.3}$$

$$\frac{\partial M}{\partial x} + V = 0 \tag{3.4}$$

Differentiating equation (3.4) with respect to x, and substituting in for $\frac{\partial V}{\partial x}$ from equation (3.3) results in

$$\frac{\partial^2 M}{\partial x^2} + \rho \frac{\partial^2 y}{\partial t^2} = 0 \tag{3.5}$$

It remains to relate the bending moment M to the transverse displacement. This fundamental relationship for a beam in bending is provided by the *moment-curvature relation*,

$$M(x,t) = EI\frac{\partial^2 y}{\partial x^2} \tag{3.6}$$

which must be satisfied for any point x along the length of the beam. Equation (3.6) is derived in [11, pp. 512-4] (see also [34, pp. 167-8] and [14, pp. 79-80]). Combining the moment-curvature relation with equation (3.5), we arrive at the governing equation

$$EI\frac{\partial^4 y}{\partial x^4} + \rho\frac{\partial^2 y}{\partial t^2} = 0 \tag{3.7}$$

for the deflections of a uniform beam in free vibration.

The solution to equation (3.7) is derived in [18, pp. 612-5] and [10, pp. 592-4]; here we simply summarize the results. The general solution can be written in the following form:

$$y(x,t) = \sum_{i=1}^{\infty} \psi_i(x) q_i(t) \tag{3.8}$$

The structure of the expression above indicates that the overall solution is composed of an infinite number of independent solutions, which we call *modal* solutions. Each term in the infinite sum defines a particular *mode of vibration* of the beam. The function $\psi_i(x)$ is termed the *mode shape* of mode i; it defines the shape that the beam assumes during vibration in that mode. The *modal amplitude* $q_i(t)$ describes how the amplitude of the associated mode shape varies over time.

The mode shapes $\psi_i(x)$ depend upon the boundary conditions of the system. For a simply supported beam, the behavior of each mode can be described by the following equations:

$$\psi_i(x) = sin\frac{i\pi x}{L} \tag{3.9}$$

$$\ddot{q}_i + {\omega_i}^2 q_i = 0 \tag{3.10}$$

$$\omega_i = \frac{i^2\pi^2}{L^2}\sqrt{\frac{EI}{\rho}} \tag{3.11}$$

where ω_i represents the *natural frequency* of vibration of mode i. From (3.9), we see that the mode shapes are sinusoids of decreasing wavelengths. The first three mode shapes are illustrated in figure 3-3.

Equation (3.10) has solutions of the form

$$q_i(t) = A_i sin(\omega_i t) + B_i cos(\omega_i t) \tag{3.12}$$

with A_i and B_i determined by initial conditions; that is, the amplitude of each mode varies sinusoidally over time, with frequency ω_i given by (3.11).

The important point to realize about the above solution is that the dynamics of various modes are entirely independent of one another. According to equation (3.10), each mode behaves like a single degree of freedom undamped oscillator; each mode is decoupled from every other mode. Equation (3.10) is termed the *modal equation of motion* of the beam.

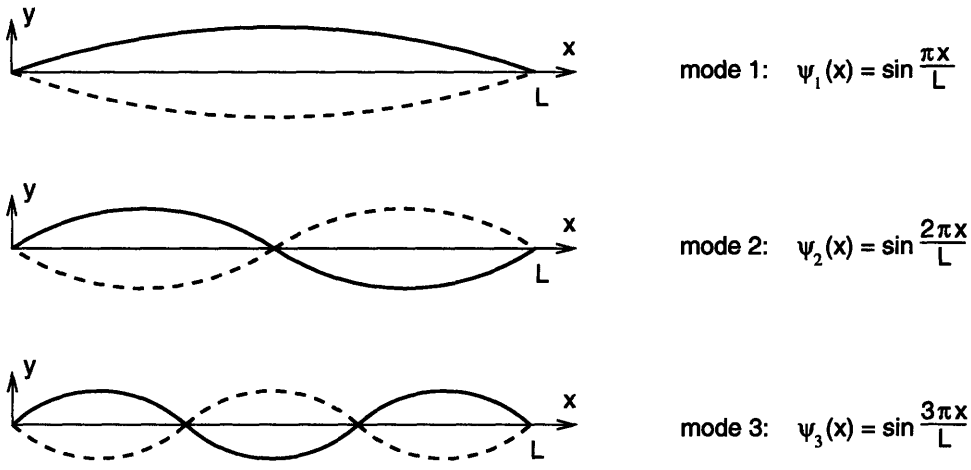

Figure 3-3: First three mode shapes of a simply supported beam.

The key property that allows us to decouple the modal equations of motion is the orthogonality of the mode shapes $\psi_i(x)$. Namely, it can be easily verified that

$$\int_0^L \psi_i(x)\psi_j(x)dx = \int_0^L sin\frac{i\pi x}{L} sin\frac{j\pi x}{L} dx = \begin{cases} 0 & i \neq j \\ L/2 & i = j \end{cases}$$

for any integer i and j. For convenience, we will also assume in our consequent analysis that the mode shapes have been normalized, such that

$$\int_0^L \psi_i(x)\psi_j(x)dx = \begin{cases} 0 & i \neq j \\ 1 & i = j \end{cases} \tag{3.13}$$

To fit equation (3.13), the mode shapes $\psi_i(x)$ must satisfy

$$\psi_i(x) = \sqrt{\frac{2}{L}} sin\frac{i\pi x}{L} \tag{3.14}$$

We will make use of the orthonormality of $\psi_i(x)$ in the analysis of section 3.3.

3.1.2 Vibration of an Axially Loaded Beam

We now consider vibration of a beam under an axial load $W(t)$. Figure 3-4 shows a differential segment of such a beam; the forces on the segment now include the longitudinal forces W applied at both ends of the segment. While the axial forces have no effect on the force equilibrium condition (3.1), the moment equilibrium condition (3.2) must be modified to include the moment induced by the applied load:

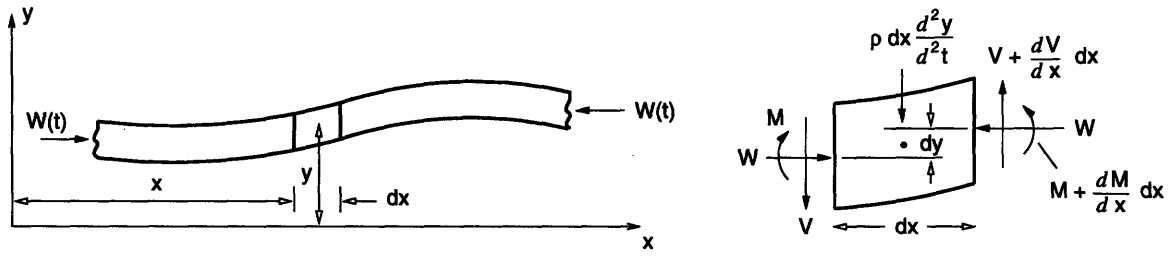

Figure 3-4: Vibration of an axially loaded beam. In addition to the shear forces and bending moments introduced in figure 3-2, each differential beam segment is subjected to longitudinal forces $W(t)$ applied at both ends of the segment.

$$(M + \frac{\partial M}{\partial x}dx) - M + (V + \frac{\partial V}{\partial x}dx)\frac{dx}{2} + V\frac{dx}{2} + Wdy = 0 \tag{3.15}$$

Simplifying this expression, as before, we obtain

$$\frac{\partial M}{\partial x} + V + W\frac{\partial y}{\partial x} = 0$$

which results in the following equation of motion for an axially loaded beam:

$$EI\frac{\partial^4 y}{\partial x^4} + W(t)\frac{\partial^2 y}{\partial x^2} + \rho\frac{\partial^2 y}{\partial t^2} = 0 \tag{3.16}$$

Comparing this expression with equation (3.7) of the beam's free vibrations, we see that they differ by the term $W(t)\frac{\partial^2 y}{\partial x^2}$, which describes an external bending moment due to the axial load $W(t)$.

How does the bending moment induced by the applied load change the behavior of a vibrating beam? It turns out that the solution of the axially loaded system (see [35, pp. 453-5], [7, p. 24]) still obeys equation (3.8), with mode shapes defined by (3.14) and modal amplitudes behaving in accordance with equation (3.10). What does change due to the applied load is the expression describing the modal frequencies of the beam's vibration:

$$\omega_i = \omega_{i_{unloaded}}\sqrt{1 - \frac{W}{W_{crit_i}}} \tag{3.17}$$

Here, $w_{i_{unloaded}}$ is given by equation (3.11), and W_{crit_i} is the *critical load* of mode i, defined as

$$W_{crit_i} \equiv \frac{i^2\pi^2 EI}{L^2} \tag{3.18}$$

Note from equation (3.17) that the modal frequencies of a loaded beam are smaller than those of a beam in free vibration. Intuitively, the bending moment applied by the axial load resists the beam's vibratory motion, and thus acts to slow it down. Furthermore, according to equation (3.17), when a beam is loaded above the critical load W_{crit_i} for some i, the frequency of vibration in mode i becomes imaginary. Physically, we interpret this to mean that the modal amplitude of mode i grows exponentially over time, leading to the collapse, or buckling, of the column.

Since the critical loads W_{crit_i} increase with increasing i, the smallest value of the load at which buckling will occur is W_{crit_1}, termed the buckling load. For an uncontrolled beam, this critical load is the only one of significance, as it represents the maximum theoretical load the beam is capable of supporting. In reality, because of imperfections in the beam and eccentricities of the applied loads, the deflections of the beam become very large even before the buckling load is reached. Thus, in practical design, the allowable load is taken to be a factor of 1.5–3 smaller than the buckling load ([34], [14]).

Through active control of the beam, we hope to stabilize the system at loads higher than the buckling load, thus increasing the beam's load-bearing strength. Below, we take a look at how this might be accomplished by discussing the dynamics of the beam subject to control forces.

3.1.3 Effect of Control Forces

The purpose of active control is to introduce new external forces in the system, thereby influencing its dynamics. For active control of buckling, several kinds of control forces are possible. For example, one could apply lateral forces along the length of the column that would push the beam in the direction of its undeflected position. Or, one could apply bending moments that would counteract the bending moment imposed by the axial load.

As we saw in chapter 2, the actuators in our system apply bending moments rather than lateral forces. Specifically, each actuator pair applies bending moments Fa at the endpoints of the corresponding segment of the beam, where F designates a longitudinal force (either tensile or compressive) applied at the endpoints of the actuators (see figure 2-6b).

For convenience of analysis, in this chapter we approximate the longitudinal forces F applied by the actuators at discrete points along the side of the beam by a continuous actuator force $F(x,t)$ applied everywhere along the side of the beam. This is essentially equivalent to assuming that the beam is covered by an infinite number of actuator pairs, each applying a unique bending moment to the corresponding differential segment of the beam. The resultant force diagram for an infinitesimal beam segment is shown in figure 3-5. For the sake of clarity, only the longitudinal forces

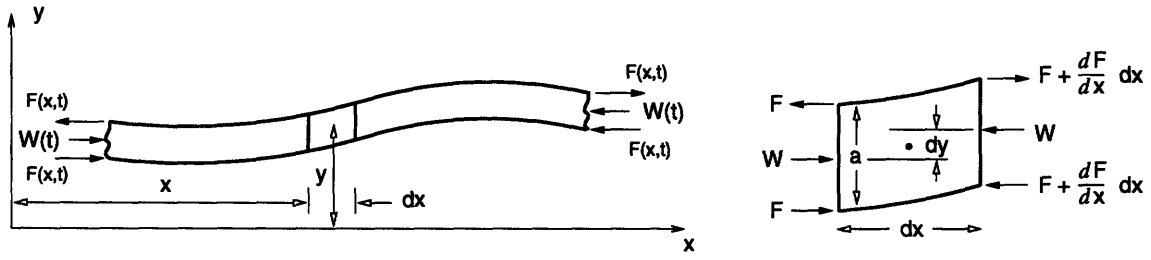

Figure 3-5: Vibration of an axially loaded beam subject to control forces. A tensile actuator force $F(x,t)$ is applied to one side of the beam, while a compressive force of the same magnitude is applied to the other side. The bending moments M, the shear forces V, and the inertial force $\rho\, dx \frac{\partial^2 y}{\partial t^2}$ are not pictured here; they are identical to the ones in figure 3-4.

are included in the diagram; the moments M due to bending, the shear forces V, and the inertial force $\rho\, dx \frac{\partial^2 y}{\partial t^2}$ are identical to the ones in figure 3-4.

In figure 3-5, the longitudinal force applied at the top of the beam segment is tensile, while the one at the bottom of the segment is compressive. The effect of these forces will thus be to push the endpoints of the segment in the negative y direction. This creates a net bending moment in the direction opposite to the bending moment applied by the axial load W. Thus, the actuator forces act to counter the bending moment due to the axial load, as desired.

We can now modify the moment equilibrium condition (3.15) to include the moments induced by the actuator force $F(x,t)$ at the endpoints of the beam segment:

$$(M + \frac{\partial M}{\partial x}dx) - M + (V + \frac{\partial V}{\partial x}dx)\frac{dx}{2} + V\frac{dx}{2} + Wdy + Fa - (F + \frac{\partial F}{\partial x}dx)\, a = 0$$

Simplification of this expression leads to

$$\frac{\partial M}{\partial x} + V + W\frac{\partial y}{\partial x} = a\frac{\partial F}{\partial x}$$

and thus to the following equation of motion for an axially loaded beam subject to the actuator forces:

$$EI\frac{\partial^4 y}{\partial x^4} + W(t)\frac{\partial^2 y}{\partial x^2} + \rho\frac{\partial^2 y}{\partial t^2} = a\frac{\partial^2 F(x,t)}{\partial x^2} \tag{3.19}$$

Comparison with equation (3.16) which holds for an uncontrolled beam reveals that influencing the beam's vibrations is now the control term $a\frac{\partial^2 F(x,t)}{\partial x^2}$. For convenience, we make the following definition:

$$U(x,t) \equiv a\frac{\partial^2 F(x,t)}{\partial x^2} \tag{3.20}$$

with which we can rewrite the equation of motion (3.19) as

$$EI\frac{\partial^4 y}{\partial x^4} + W(t)\frac{\partial^2 y}{\partial x^2} + \rho\frac{\partial^2 y}{\partial t^2} = U(x,t) \tag{3.21}$$

We will often refer to $U(x,t)$ as the control force, but it should be kept in mind that it does not correspond directly to the actuator forces being applied.[2]

The solution to equation (3.21) (see [26, pp. 452-3]) tells us how the control force influences the dynamics of the beam. As before, the general solution of the system satisfies equation (3.8), with mode shapes defined by (3.14). However, the modal equations of motion are affected by the presence of the control force $U(x,t)$:

$$\ddot{q}_i + {\omega_i}^2 q_i = \frac{u_i(t)}{M_i} \tag{3.22}$$

where the *modal force* $u_i(t)$ and the *modal mass* M_i are given by

$$u_i(t) = \int_0^L U(x,t)\psi_i(x)dx \tag{3.23}$$

$$M_i = \int_0^L \rho\psi_i^2(x)dx = \rho \tag{3.24}$$

(The simplification in equation (3.24) is due to the orthonormality of the mode shapes, equation (3.13).) The modal force $u_i(t)$ should be interpreted as the portion of the applied control force $U(x,t)$ which excites mode i, and the modal mass M_i can be thought of as a mass-like quantity. In addition, we define the *modal stiffness* K_i as

$$K_i = M_i{\omega_i}^2 = \rho{\omega_i}^2 \tag{3.25}$$

Modal stiffness is essentially the spring constant of the harmonic oscillator described by equation (3.22): high K_i implies a high restoring force in an event of deflection in mode i.

The modal frequencies ω_i in equation (3.22) are given by (3.17), as in the case of an uncontrolled (but loaded) beam. Equation (3.22) has a homogeneous solution,

[2]There is another reason for making the definition (3.20) besides convenience; it allows us to treat the control term present in the equation of motion as an abstract force $U(x,t)$, not specific to the particular kind of forces being applied. For example, it turns out that if the actuator force $F(x,t)$ were lateral rather than longitudinal, the control term $U(x,t)$ would be defined simply as $F(x,t)$ rather than $a\frac{\partial^2 F(x,t)}{\partial x^2}$.

given by (3.12), as before, and a particular solution, which depends on the modal force $u_i(t)$ and thus on the applied control force $U(x,t)$.

Note that, in spite of the changes in the system introduced by the applied forces, the form of the solution remains the same: the forced vibrations of the beam are still determined by the vibrations of the mode shapes $\psi_i(x)$. Different modes are again decoupled from each other, as demonstrated by equation (3.22); each mode still behaves like a single degree of freedom undamped oscillator, this time subjected to a force $u_i(t)$.

We can now see how active control allows us to prevent the beam from buckling. Recall that, when an uncontrolled beam is put under an axial load in excess of the critical load for some mode i, the associated modal frequency ω_i becomes imaginary, leading to the collapse of the column. In the case of a controlled beam, however, equation (3.22) reveals that the quantity ω_i does not necessarily represent the actual frequency of mode i. For example, if we arrange for the modal force to be proportional to the modal amplitude, $u_i(t) = -kM_iq_i(t)$ for some positive k, the frequency of vibration in mode i becomes $\sqrt{\omega_i^2 + k}$, a quantity that can be kept real even if ω_i is imaginary. Another way to say this is that the effective modal stiffness, $K_i + kM_i$, can be kept positive, providing a restoring force necessary to counteract the deformations in mode i. Thus, theoretically it is possible to prevent buckling in any mode i by applying an appropriate stabilizing modal force $u_i(t)$.

In practice, it is clear from equation (3.18) that the modes that require active control the most are the lowest ones: with no control, the beam can support some maximum axial load W_{crit_1}; with the first mode controlled, the value of the maximum load that can be supported is increased by a factor of 4 to $W_{crit_2} = 4W_{crit_1}$; with the first two modes controlled, the maximum load is $W_{crit_3} = 9W_{crit_1}$; and so on. Preventing buckling in the first n modes will theoretically result in a factor of $(n+1)^2$ increase in the load-bearing strength of the beam.

3.2 Modal and Local Control

So far in our discussion of the controlled beam dynamics, we have been treating the control forces as abstract quantities (or functions) that vary depending on the control law being used. It is now time to specify the control forces applied by the two particular controllers of interest, modal and local.

Notice that there are two domains in which the control forces can be specified—physical and modal. In the physical domain, the behavior of the beam is modeled by equation (3.19), describing the physical deflection of the beam over time; the control force contained in equation (3.19) is the physical force $F(x,t)$ applied by the actuators. In the modal domain, the beam's vibrations are instead expressed in terms of an infinite number of modes, with each mode obeying the modal equation of motion (3.22); the control force for each mode i, contained in equation (3.22), is the modal force $u_i(t)$. Since the descriptions of the beam dynamics in the physical and modal domains are equivalent, control design can take place in either of the two domains. Below, we shall see that the local controller operates in the physical domain,

and the modal controller—as its name implies—in the modal domain.

3.2.1 Modal Control

We saw earlier in this chapter that the modal equations of motion of the beam, (3.22), are independent of one another, such that each mode of vibration is decoupled from every other mode. One natural and direct way of influencing the beam's vibrations, therefore, is to design an independent controller for each mode of the system. This is the principle of modal control (see [33], [22], [5]).

While, theoretically, the beam possesses an infinite number of modes, in practice, not all of them need to be controlled. We saw in section 3.1.2 that for buckling control, the low modes are critical: preventing buckling in the lowest n modes theoretically results in a factor of $(n+1)^2$ increase in the load-bearing strength of the beam. Thus, even for small n, buckling control of the first n modes yields a dramatic improvement in the system's performance. We therefore assume in the following that under modal control, only the lowest n modes of the beam are controlled.

As mentioned above, the control forces under modal control are specified in the modal domain. For each mode $i = 1, \ldots, n$, the control force $u_i(t)$ is given by

$$u_i(t) = P_i q_i(t) + D_i \dot{q}_i(t) \tag{3.26}$$

That is, a PD control law (see equation (2.2)) is implemented for each mode i, with the proportional and derivative gains P_i and D_i independent of the gains of any other mode. The state of the system is represented by the modal amplitudes $q_i(t)$ and the modal velocities $\dot{q}_i(t)$. The goal of the controller is to keep $q_i(t)$ close to zero: note that the beam is in the desired (straight) position when $q_i(t) = 0$ for all i.

Of course, while the controller can be designed in the modal space, the system must operate in the physical space. Thus, the modal controller must convert between the two domains. Specifically, the strain readings obtained by the sensors have to be converted to the modal amplitudes and velocities to be fed into the control law. Likewise, the desired modal forces calculated by the control law have to be converted back to the actuator forces to be applied.

To see how strain readings can be used to obtain the modal information required by the control law, first recall from equation (2.1) that the sensor reading at point x along the length of the beam is related to the deflection y at that point via the second derivative. For the purposes of this chapter, let us approximate the strain readings measured at discrete points along the side of the beam by a continuous function $s(x,t)$. (We made an analogous assumption when we approximated the discrete actuator forces by a continuous force $F(x,t)$.) This is equivalent to assuming that the beam is covered by an infinite number of sensor pairs, each supplying a unique strain measurement for the corresponding differential segment of the beam. Modifying equation (2.1) to reflect the dependence of the sensor information on time as well as space, we obtain the following expression for the strain measured everywhere along the length of the beam:

$$s(x,t) = -a\frac{\partial^2 y}{\partial x^2} \tag{3.27}$$

Thus, at a particular point in time t, the strain $s(x,t)$ along the beam can be converted to the deflection $y(x,t)$ via double integration. The deflection, on the other hand, is related to the modal amplitudes $q_i(t)$ via equation (3.8). Therefore, to convert from strain readings to modal amplitudes, we can first use the strain information to find the deflection of the beam, and then decompose $y(x,t)$ into the modal coordinates $q_i(t)$.

Similarly, the actuator force $F(x,t)$ can be recovered from the modal forces $u_i(t)$ via equations (3.23) and (3.20). We will not linger on the details of this operation here, but will instead come back to describe both transformations in chapter 4, when discussing the modal controller implementation.

It is clear from the above that modal control satisfies our definition of a global, or centralized, control approach. First, it makes explicit use of a global model of the system, described by the modal equations of motion of the beam, (3.22). Secondly, it requires global sensor information in order to calculate control actions: as we saw above, the modal amplitudes $q_i(t)$ are obtained given the strain readings along the entire length of the beam.

3.2.2 Local Control

In contrast to modal control, local control assumes no knowledge of the global properties of the system; the control depends strictly on local information at each point along the beam. In particular, we use the sensor information itself (i.e., the strain $s(x,t)$) as the basis of local control. The task of the controller is to keep the strain everywhere along the beam close to zero; this is a reasonable goal, as small strain (which is proportional to curvature $\frac{\partial^2 y}{\partial x^2}$, see equation (3.27)) also ensures small deflection. The output of the control law is the physical actuator force $F(x,t)$:

$$F(x,t) = Ps(x,t) + D\frac{\partial s(x,t)}{\partial t} \tag{3.28}$$

Note that at each point x along the beam, the control force $F(x,t)$ is determined based only on the strain $s(x,t)$ measured at that point and its time derivative. Since the beam is assumed to be uniform, the same control gains P and D are used to calculate the control forces everywhere on the beam.

While equation (3.28) assumes continuous sensing and actuation everywhere along the length of the beam, it is easy to see how the local control law can be discretized to accommodate a real system with only a finite number of sensors and actuators. As described in chapter 2, our system employs a total of 10 sensors and 10 actuators, with each set of two sensors and two actuators collocated at some position along the beam. For each set $i = 1, \ldots, 5$ of two sensors and two actuators, let $s_i(t)$ be the

strain measured at the location of the sensors, and let $F_i(t)$ be the force exerted by the corresponding actuators. Then, the control law is defined for each i as follows:

$$F_i(t) = Ps_i(t) + D\dot{s}_i(t) \tag{3.29}$$

We will use this discrete version of local control for the controller implementation in chapter 4. In the analysis of this chapter, however, we will find it more convenient to stick to the continuous control law, (3.28).

Even without going into the details of controller implementation, it is clear that local control is much easier to implement that modal control. Since the local controller operates in the physical space, no conversions are required between the physical and modal domains. In fact, no global model of the system is utilized at all: instead, the system is decomposed into a number of local subsystems, which operate strictly on the basis of local sensor measurements. In addition, because the subsystems are independent of one another, multiple computational units can be used to handle control of small local regions of the structure, simplifying the tasks of data collection, processing, and distribution.

3.3 Analysis

Our discussion of the modal and local controllers culminates in this section with the analysis and comparison of the behavior of the system subject to the two kinds of control.

While equations (3.26) and (3.28) describe the control forces used by the modal and local controllers, the two expressions cannot be easily compared, as the control forces are specified in different domains. To put the two control laws on an equal footing, we need to convert one of these expressions to the domain of the other. We saw in section 3.1 that generally, more insight can be gained into the system's behavior by studying the equations of motion in the modal, rather than the physical, domain. Therefore, our strategy is to first derive an expression describing the modal forces $u_i(t)$ corresponding to the physical control force $F(x,t)$ applied by the local controller, and then analyze the modal behavior of the system under both kinds of control.

3.3.1 Modal Forces Applied via Local Control

Converting from the actuator force $F(x,t)$ exerted by the local controller (equation (3.28)) to the corresponding modal forces $u_i(t)$ is simply a matter of performing a series of algebraic manipulations. The general approach is to first combine equations (3.28) and (3.20) to obtain an expression for the control force $U(x,t)$, and then use equation (3.23) to convert $U(x,t)$ to the modal forces $u_i(t)$.

We start by expanding equation (3.28), substituting for the strain $s(x,t)$ from equation (3.27):

$$F(x,t) = -Pa\frac{\partial^2 y}{\partial x^2} - Da\frac{\partial}{\partial t}\left(\frac{\partial^2 y}{\partial x^2}\right)$$

Next, we substitute $F(x,t)$ into equation (3.20) to obtain an expression for the control force $U(x,t)$:

$$\begin{aligned} U(x,t) &= a\frac{\partial^2 F(x,t)}{\partial x^2} \\ &= -a^2 P\frac{\partial^4 y}{\partial x^4} - a^2 D\frac{\partial}{\partial t}\left(\frac{\partial^4 y}{\partial x^4}\right) \end{aligned} \tag{3.30}$$

The term $\frac{\partial^4 y}{\partial x^4}$ in the expression above can be expanded further: with y given by equation (3.8), we differentiate four times with respect to x to obtain

$$\frac{\partial^4 y}{\partial x^4} = \sum_{i=1}^{\infty} \frac{d^4\psi_i}{dx^4} q_i(t) \tag{3.31}$$

With the mode shapes $\psi_i(x)$ of a uniform simply supported beam given by equation (3.14), we have, for each mode i,

$$\frac{d^4\psi_i}{dx^4} = \frac{d^4}{dx^4}\left(\sqrt{\frac{2}{L}}sin\frac{i\pi x}{L}\right) = \left(\frac{i\pi}{L}\right)^4\left(\sqrt{\frac{2}{L}}sin\frac{i\pi x}{L}\right) = \left(\frac{i\pi}{L}\right)^4\psi_i(x)$$

Substituting back into equation (3.31) yields

$$\frac{\partial^4 y}{\partial x^4} = \left(\frac{\pi}{L}\right)^4 \sum_{i=1}^{\infty} i^4\psi_i(x)q_i(t)$$

At last, the above expression is substituted into equation (3.30) to obtain the following expression for the control force $U(x,t)$:

$$\begin{aligned} U(x,t) &= -a^2 P\left(\frac{\pi}{L}\right)^4 \sum_{i=1}^{\infty} i^4\psi_i(x)q_i(t) - a^2 D\left(\frac{\pi}{L}\right)^4 \frac{\partial}{\partial t}\left(\sum_{i=1}^{\infty} i^4\psi_i(x)q_i(t)\right) \\ &= -a^2 P\left(\frac{\pi}{L}\right)^4 \sum_{i=1}^{\infty} i^4\psi_i(x)q_i(t) - a^2 D\left(\frac{\pi}{L}\right)^4 \sum_{i=1}^{\infty} i^4\psi_i(x)\dot{q}_i(t) \end{aligned}$$

The modal forces $u_i(t)$ can now be found by substituting $U(x,t)$ into equation (3.23). The result is

$$
\begin{aligned}
u_i(t) &= \int_0^L U(x,t)\psi_i(x)dx \\
&= -a^2P\left(\frac{\pi}{L}\right)^4 \int_0^L \left(\sum_{j=1}^{\infty} j^4\psi_j(x)q_j(t)\right)\psi_i(x)dx \\
&\quad - a^2D\left(\frac{\pi}{L}\right)^4 \int_0^L \left(\sum_{j=1}^{\infty} j^4\psi_j(x)\dot{q}_j(t)\right)\psi_i(x)dx
\end{aligned}
$$

Because of the orthonormality condition (3.13), however, most of the terms in both sums above disappear, leaving

$$
u_i(t) = -a^2P\left(\frac{\pi}{L}\right)^4 i^4 q_i(t) - a^2D\left(\frac{\pi}{L}\right)^4 i^4 \dot{q}_i(t) \tag{3.32}
$$

For convenience, we define new constants $\tilde{P}$ and $\tilde{D}$ as follows:

$$
\begin{aligned}
\tilde{P} &\equiv -a^2P\left(\frac{\pi}{L}\right)^4 \\
\tilde{D} &\equiv -a^2D\left(\frac{\pi}{L}\right)^4
\end{aligned}
$$

Incorporating these constants into equation (3.32) finally produces

$$
u_i(t) = \tilde{P}i^4 q_i(t) + \tilde{D}i^4 \dot{q}_i(t) \tag{3.33}
$$

3.3.2 Modal vs. Local Control

We are now ready to compare modal and local control based on the two expressions for modal control forces, equations (3.26) and (3.33), reproduced here for convenience:

$$
\begin{aligned}
u_{i_{modal}}(t) &= P_i q_i(t) + D_i \dot{q}_i(t) \\
u_{i_{local}}(t) &= \tilde{P}i^4 q_i(t) + \tilde{D}i^4 \dot{q}_i(t)
\end{aligned}
$$

Note, first of all, that the two expressions above have the same basic structure, characteristic of PD controllers: in both cases, the control action for each mode i consists of a proportional and a derivative term. Recall from section 3.1.3 that the proportional term modifies the frequency of vibration in mode i, making it possible to keep the beam from buckling in mode i even if the axial load exceeds the critical load W_{crit_i}. The derivative term acts to damp out the oscillations in mode i, described by equation (3.12). Together, these two terms can be used to stabilize mode i of the beam in the face of disturbances.

The difference between the expressions for $u_{i_{modal}}$ and $u_{i_{local}}$ lies in the gains of the modal control forces. Taking proportional gain as an example, we see that in modal control, the gain P_i for mode i is independent of the gains for all the other modes. In contrast, in the case of local control, the proportional gain for mode i depends both on the globally set quantity $\tilde{P}$ and on the mode number i. The situation is identical with respect to the derivative gains.

Before diving into the implications of these gain values on modal and local control, let us briefly discuss the question of how the values of PD control gains affect system performance. Intuitively, we expect that a higher proportional gain would produce a greater corrective action, while a higher derivative gain would introduce a higher damping term; together, these higher gains would lead to faster stabilization of the system. Thus, higher gains for a particular mode i result in more *control authority* dedicated to mode i. Note also that greater control authority comes at a greater expense, as it generates stronger actuation signals.

We have observed previously that in buckling control, it is more important to stabilize the low modes rather than the high ones; for example, our design objective could be to stabilize the lowest n modes of the system, so as to provide an $(n+1)^2$ increase in the load-bearing capability of the beam. As the preceding paragraph indicates, this calls for high control gains for the first n modes of the system, and low (or zero) gains for all the other modes. Note also that, the lower the mode is, the more vital its stabilization is to the stability of the entire system, and the more important it is to provide it with high control authority.

Keeping this in mind, we now return to the comparison of the modal and local controllers. In modal control, since the control gains P_i and D_i for mode i are independent of the gains for all the other modes, the control designer has complete freedom in varying the gains for a particular mode without affecting the behavior of other modes. In particular, we can set the gains for low modes to be high, and the gains for high modes to be low, as desired. (In fact, we already assumed in section 3.2.1 that only the first n modes have non-zero gains.) That is to say, modal control allows for optimal settings of the control gain values.

In local control, on the other hand, the control gains for mode i cannot be independently set; rather, we see from the expression for $u_{i_{local}}$ that the gains increase with increasing i. This leads to greater control authority being dedicated to higher modes. Thus, under local control, the higher the mode is, the more effort will be spent on its stabilization, and the faster it will get stabilized. This may present a problem in the face of limitations on the amount of total control authority available (i.e., limited actuator strength): with most of the control authority dedicated to the high modes, the low modes will exhibit a more sluggish response. Subjected to a large disturbance, the system may not be able to react to the low frequency deflections quickly enough, leading to further destabilization of the low modes and eventual collapse of the beam.

In spite of this apparent handicap, there are several factors that prevent us from dismissing local control as an inferior control strategy. First of all, precisely because higher modes have greater control authority, their stabilization proceeds very quickly. As the high modes are stabilized, their modal amplitudes $q_i(t)$ and velocities $\dot{q}_i(t)$ become very small, yielding correspondingly small modal forces $u_i(t)$. As a result,

the control authority initially used to stabilize the high modes is soon redirected to the lower modes.

In addition, it turns out that the effect described above is even more significant due to inherently high stiffness associated with the higher modes. We can see from equation (3.25) that the modal stiffness K_i goes up as the square of the modal frequency ω_i; furthermore, equations (3.17) and (3.11) indicate that the modal frequency itself is proportional to the square of the mode number, i.[3] Thus, the modal stiffness K_i varies as i^4. Any deflections in mode i are counteracted by a restoring force commensurate to the modal stiffness K_i. Combined with the high control authority (also proportional to i^4), this restoring force assures quick stabilization of the high frequency mode.

Considering the effects of stiffness from a slightly different angle, we see that in fact the amount of modal stiffness is directly related to how easy or difficult it is to excite the associated mode. For example, it is more difficult to bend a column in the shape of mode 2 than it is to bend the same column in the shape of mode 1; the physical explanation for this phenomenon is precisely the higher stiffness associated with mode 2. The higher the mode, the more it resists destabilization, and the more force, or energy, is required to generate a deflection in that mode. Therefore, higher modes are not only easier to stabilize once they are excited, but they are more difficult to excite in the first place. As a result, the amplitudes of the high frequency modes are typically very small, and thus only require little control authority (we will see the evidence of this in chapter 5, when we look at the real modal data taken from the prototype beam). In effect, most of the available control authority is used to stabilize the lower modes, as desired.

The upshot of all this is that the handicap exhibited by local control in equation (3.33) is not nearly as severe as it might first appear. Although we do not have the freedom, as we do in modal control, to arbitrarily set the control gains in order to satisfy our goals, the crude analysis presented here indicates that, theoretically at least, the gains actually used in local control could yield performance approaching that achieved by the modal controller. We will see quantitative results confirming this conclusion in chapters 4 and 5.

3.4 Caveats

Throughout this chapter, we have made several idealizing assumptions in order to simplify the analysis of the behavior of the beam under active control. Our purpose has been to develop intuition, and to state general qualitative results, rather than to stay precise; more accurate models of the system, as well as real experimental data, are presented later on in the thesis. As a result, some of the assumptions made in this chapter are not very accurate for the real system under consideration. Deviations

[3] We are assuming that for the mode under consideration, $W \ll W_{crit_i}$; in that case, $\omega_i \approx \omega_{i_{unloaded}} \propto i^2$. This condition is easily satisfied even for relatively small i, given the typical axial loads used in the system.

from the ideal conditions assumed in our analysis may result in differences in behavior between the idealized system considered here and the real system at hand.

We assumed early on in the chapter that the beam is uniform; this lead to substantial simplifications of the equations of motion presented in section 3.1. We saw in chapter 2, however, that the real beam does not have uniform material properties over its entire length: for example, actuators add to the thickness of those segments of the beam which they cover. On the other hand, the assumption of uniformity does not seem unreasonable given the particular structure of the prototype column, especially considering the implications for the ease of analysis.

Approximating the discrete sensor readings and actuator forces by their continuous equivalents, $s(x,t)$ and $F(x,t)$, allowed us to derive the equations of motion of a beam subject to control forces, and to specify the control forces exerted by the modal and local controllers. In a real system, of course, sensing and actuation are performed at discrete points along the length of the beam. In addition, real control is not performed instantaneously, as we implicitly assumed here: both sensing and actuation occur at discrete time intervals, corresponding to the sampling frequency of the controller. In the simulations described in chapter 4, we take all of these issues into account by providing the simulated system with a finite number of sensors and actuators, as well as a finite sampling rate.

Another simplification made in this chapter that we do away with in chapter 4 is the absence of sensor noise in the system. The errors due to measurement noise may result in degraded performance of the controllers.

Lastly, the introduction of modal control in section 3.3 contained a brief description of the conversions between the modal and physical domains required in the implementation of the modal controller. In the subsequent analysis, we assumed that these conversions could be performed in a way that would allow no information to be lost as a result of the transformations. As we discover in chapter 4, however, this assumption was in fact unjustified. As it turns out, the information lost in the process of converting between the modal and local domains is one of the most important factors limiting the performance of modal control. We explore the implications of this limitation in detail in chapter 4.

Chapter 4

Simulation

This chapter describes computer simulations performed in order to evaluate the relative performance of the modal and local control strategies. We start by describing the simulator built for this purpose. We then describe the implementation of both local and modal control laws, and present the results of the simulations performed.

4.1 The Simulator

The simulation of beam dynamics requires essentially that we integrate the equations of motion of the beam over time. We have seen in chapter 3 that the beam's vibrations can be described in two ways: either by the partial differential equation (PDE) (3.21) in which the displacement $y(x,t)$ of any point on the beam is a function of both its position along the beam and time, or by the modal equations of motion (3.22).[1] The advantage of the modal space representation is that the modal amplitudes q_i are functions of time only; thus, equations (3.22) are second-order linear ordinary differential equations (ODEs), which turn out to have exact analytic solutions. Therefore, by simulating in modal space, we can avoid dealing with the problems associated with integrating the PDE numerically.

In theory, an infinite number of modal equations is required to accurately represent the deflection of the beam. However, as in chapter 4, we can again take advantage of the fact that high modes are more difficult to excite than low ones. In practice, therefore, we can get away with simulating only the lowest few modes of vibration of the beam, and assuming zero amplitudes for the higher modes.

Even with these simplifications, however, some problems remain. One consequence of simulating in the modal domain is that we have to convert between the modal representation used by the simulator and the physical representation (of measured strains and applied actuator forces) employed by the controllers. The modal forces $u_i(t)$, for example, can be obtained from the control force $U(x,t)$ by integrating over the length of the beam, as in equation (3.23). Note, however, that in chapter 3

[1] Note that neither of these equations contains a damping term. As a rule, in simulating structural dynamics, damping is either neglected or estimated through physical measurements. We choose to neglect it.

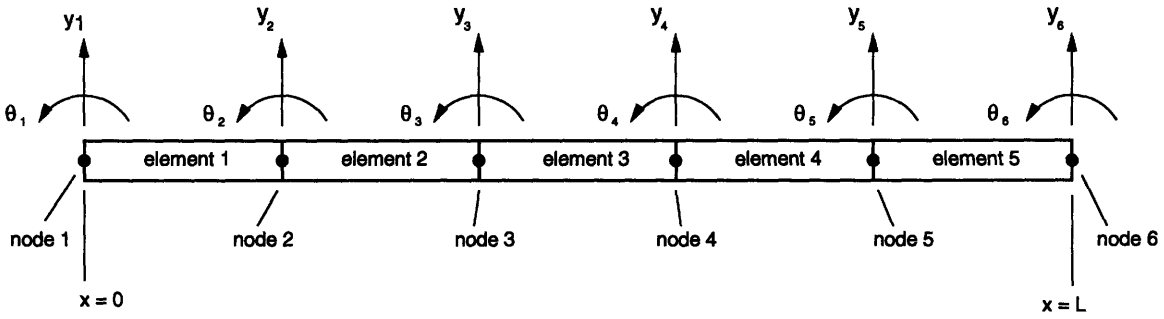

Figure 4-1: Discretization of beam coordinates via finite element method. The beam is broken up into 5 equal-length elements, and the 6 points at which the elements meet are identified as nodes. With two coordinates, y_i and θ_i, given to each node i, FEM yields a system with 12 nodal coordinates.

the actuator force $F(x,t)$ (and thus, the control force $U(x,t)$) was assumed to be continuous over the length of the beam. In reality, of course, as discussed in chapter 2, the control forces are very much discrete: in effect, each of the five actuators applies bending moments only at its endpoints.

To facilitate the conversion between the modal and physical domains, we make use of the *finite element method* (FEM). For the past 20 or 30 years, FEM has been the most common way to analyze the dynamics of complex structures ([4], [10]). In its most general form, FEM allows one to model a structure as an arbitrary collection of discrete elements, each with its own mass and stiffness properties. The formulation of the finite element method, and its application to the analysis of beam dynamics, for the case of the prototype beam, is briefly discussed below.

4.1.1 Finite Element Method

This section reviews the finite element method for the case of forced vibration of a uniform beam in one dimension. As argued in chapter 4, the assumption of a uniform beam is not unreasonable in our case: although sensing and actuating devices affect the material properties of the beam, they do so in a roughly uniform fashion. For a more complete treatment of FEM, see [10, section 9.6], where this particular example is worked out in detail.

FEM starts by breaking the beam up into discrete segments, or *elements*. The points at which the elements meet are called *nodes*, and each node i has associated with it a vertical displacement y_i and a rotation angle θ_i, as shown in figure 4-1 (for small displacements, which are assumed here, the rotation angle is simply the slope y_i' of the displacement). In our case, the beam is broken up into 5 equal-length elements, corresponding to the 5 actuators. Thus, we obtain a system with 12 *nodal coordinates*, $y_1, \theta_1, \ldots, y_6, \theta_6$. Note that, because the nodal coordinates are identified with specific locations along the beam, they are functions of time only and not of space.

We now approximate the shape of each of the elements by a cubic polynomial, subject to four boundary conditions provided by the nodal values of the two adjacent

nodes. As a result, we effectively obtain an approximation to the displaced shape $y(x,t)$ of the entire beam in terms of the nodal values $y_1(t), \theta_1(t)$ through $y_6(t), \theta_6(t)$. The exact shape functions used in the above approximations are given in [10, section 9.6.2].

So far, our finite element approximation takes no account of the underlying physical model of the system at hand: it is simply a geometric construction. The next step is to derive, based on the governing equation of motion, equation (3.21), the differential equations that describe the time dependence of the nodal coordinates $y_i(t)$ and $\theta_i(t)$. Notice that, while equation (3.21) is a PDE, the discrete element model will yield ODEs, since the nodal coordinates are functions of time only. The method used to obtain the finite element equations of motion of the beam utilizes Lagrange's equations, and is described in detail in [10, section 9.6.3]. The result is the following system of ordinary differential equations:

$$[M]\{\ddot{y}\} + [K]\{y\} = \{U\} \tag{4.1}$$

Here, $\{y\}$ is a column vector of nodal displacements, $y_1(t)$ through $\theta_6(t)$, and $\{\ddot{y}\}$ is the corresponding vector of their second derivatives with respect to time. The column vector $\{U\} = [U_{y_1}\ U_{\theta_1}\ \ldots\ U_{y_6}\ U_{\theta_6}]^T$ represents the *nodal forces*, or the forces that affect the associated nodal values. For example, U_{y_1} represents the lateral force applied at node 1, and U_{θ_1} describes the bending moment applied at the same node. Thus, we see that the finite element formulation allows us to express the discrete bending moments applied by the actuators at their endpoints in a natural fashion.

Finally, the mass and stiffness matrices, $[M]$ and $[K]$, describe the mass and stiffness properties of the system modeled by discrete elements. Roughly speaking, the beam is being treated as a collection of discrete particles situated at the nodal points, connected by springs; the mass and stiffness properties of the beam are associated with these discrete particles and the springs between them. The matrices $[M]$ and $[K]$ are derived in [10] for the case of a uniform beam.

Note that the above formulation does not take into account the boundary conditions of the system in question. For the case of a simply supported beam, boundary conditions dictate that we must have $y_1 = y_6 = 0$ for all time. This restriction eliminates 2 of the 12 nodal coordinates, reducing the dimension of the system (4.1) to 10. The mass and stiffness matrices are modified appropriately, by getting rid of the rows and columns corresponding to the eliminated coordinates.

To summarize, what we have done with finite elements is to convert the problem of analyzing a *continuous* system to a (generally easier) problem of analyzing what is called a *discrete, multiple degree of freedom* (multi-DOF) system. Using this discrete formulation, we can now naturally express sensing and actuation as being performed at discrete points along the beam. In the process of transforming the continuous PDE into the multi-DOF system of equations, however, what have we done to the modal equations of motion? It turns out that the modal equations for the multi-DOF systems parallel closely those for the continuous systems. The results are summarized in the next section.

4.1.2 Modal Equations of Motion for a Multi-DOF System

For modal equations of motion describing a multi-DOF system, we refer to [10, section 7.3.3]. Let n be the order of the system (in our case, $n=10$, for our system is described in terms of 10 nodal coordinates). Then, for each mode $i = 1, \ldots, n$,

$$\ddot{q}_i + {\omega_i}^2 q_i = \frac{u_i(t)}{M_i} \tag{4.2}$$

where

$$u_i(t) = \{C\}_i^T \{U\} \tag{4.3}$$

$$M_i = \{C\}_i^T [M] \{C\}_i \tag{4.4}$$

Note the close correspondence between equations (4.2)–(4.4) and equations (3.22)–(3.24). The difference is that, instead of functions $U(x,t)$, ρ, and $\psi_i(x)$, which are continuous along the length of the beam, our new modal equations feature discrete approximations to those functions—namely, $\{U\}$, $[M]$, and $\{C\}_i$, respectively. Notice, in addition, that the above equations only hold for the first n modes of the system. The higher modes are not included in the approximation.

The discrete mode shapes $\{C\}_i$ are n-element column vectors which represent approximations to the true mode shapes $\psi_i(x)$, as expressed in nodal coordinates. To determine $\{C\}_i$, we solve the homogeneous system

$$[M]\{\ddot{y}\} + [K]\{y\} = \{0\} \tag{4.5}$$

More specifically, we assume the solution

$$\{y(t)\} = \sum_{i=1}^{n} \{C\}_i q_i(t) \tag{4.6}$$

(compare to equation (3.8)), with q_i described by equation (3.12), as before. Substituting this into (4.5), we find that the mode shapes $\{C\}_i$ are the eigenvectors of the matrix $[M]^{-1}[K]$, with the associated eigenvalues given by the squares of the modal frequencies, ${\omega_i}^2$. Thus, the approximate mode shapes and the corresponding approximate frequencies are found by solving the algebraic eigenvalue problem defined in terms of the system's mass and stiffness matrices.

We are now ready to describe the conversions between the modal domain used by the simulator and the physical domain employed by the control laws. Let us first take a closer look at equation (4.6). It says that, at any time t, the displacement of the beam $\{y(t)\}$ can be represented as a superposition of the n mode shapes; the contribution of a given mode $\{C\}_i$ to the overall displacement pattern is defined by the instantaneous value of the associated modal amplitude $q_i(t)$. We can rewrite this

more concisely as

$$\{y\} = [C]\{q\} \tag{4.7}$$

where $\{q\}$ is the column vector of modal coordinates q_i, and the *modal matrix* $[C]$ is the matrix of mode shapes,

$$[C] = [\{C\}_1\{C\}_2 \ldots \{C\}_n]$$

Equation (4.7) gives us an easy, convenient way to transform from the modal amplitudes to the physical displacement of the beam (expressed in terms of nodal coordinates). The inverse transformation can be accomplished by simply inverting the modal matrix.

We will also need to convert between modal and applied forces. Toward that end, we rewrite equation (4.3) as

$$\{u\} = [C]^T\{U\} \tag{4.8}$$

where $\{u\}$ is the column vector of modal forces $u_i(t)$. Once again, the inverse operation is accomplished by inverting the matrix of linear transformation.

Let us step back for a moment and evaluate what we have done. Using the finite element method, we transformed a continuous system of chapter 3 into its discrete approximation—a multi-DOF system of order n. The discrete system, described in the physical domain by equation (4.1) and in the modal domain by equations (4.2)–(4.4), is completely analogous to the continuous system; we could have easily used the discrete version in our analysis of chapter 3, for example, with equivalent results. The advantage provided by the discretized system is two-fold. First, it allows us to naturally express, using nodal coordinates, both the strains measured and the bending moments applied at discrete points along the beam. Second, it lets us frame the conversions between modal and physical domains as simple linear transformations, equations (4.7) and (4.8). In the next section, we will see how the simulator makes use of these transformations.

How accurate is our discrete approximation? We have already noted that only the first n modes of vibration are included in the multi-DOF system. For those n modes, discrepancies exist between the exact and the approximate mode shapes, as well as the exact and the calculated natural frequencies. As a rule of thumb, it is usually assumed that approximately the first $n/2$ of n modes are determined accurately using FEM, with more substantial discrepancies observed for the last $n/2$ modes ([10, p. 611]). In our case, this means that the first 5 modes are represented accurately; this was deemed acceptable for our purposes.

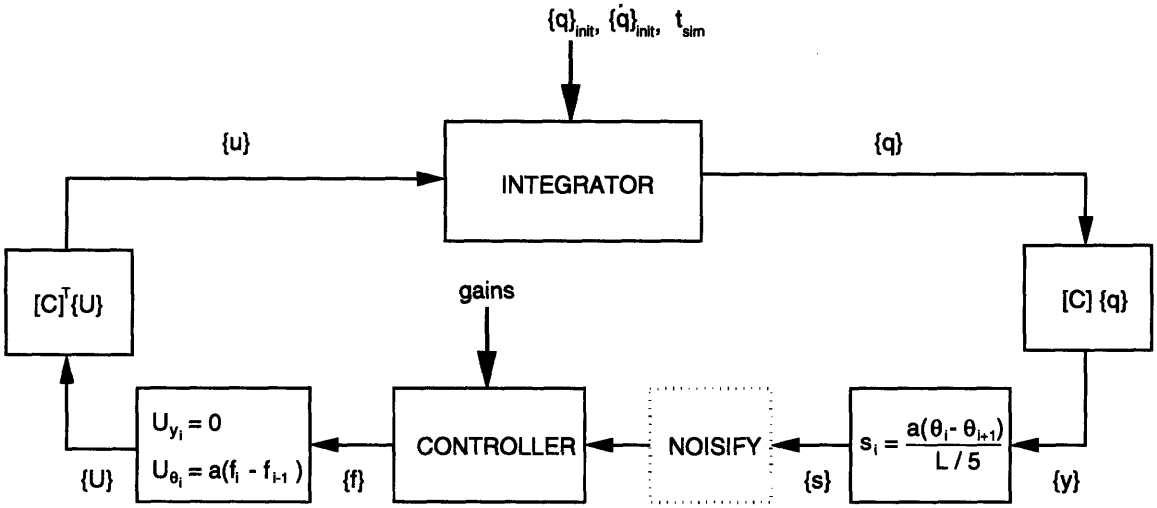

Figure 4-2: The flow of data through the simulator. The main components of the simulator are the integrator and the controller. Given the strain readings $\{s\}$, the controller produces the actuator forces $\{f\}$, which are converted to modal forces $\{u\}$. Based on the modal forces thus applied, the integrator calculates the next modal state of the system, represented by the modal amplitudes and velocities, $\{q\}$ and $\{\dot{q}\}$. The modal amplitudes are then converted to strains (which can undergo optional "noisification"), and the process repeats. The inputs to the simulator include the initial modal state, $\{q\}_{init}$ and $\{\dot{q}\}_{init}$, and the duration of the run, t_{sim}. In addition, the user must specify the control gains to be used by the controller.

4.1.3 The Workings of the Simulator

We can now turn to the discussion of the simulator itself. The flow of information through the simulator is shown schematically in figure 4-2.

The two main components of the simulator are the integrator and the controller. In this section, we treat the controller as a black box that simply takes in 5 strains measured by the sensors and outputs 5 actuator forces, one for each actuator pair. The integrator is then responsible for simulating the effects of the actuator forces thus applied. The innards of two types of controllers, local and modal, will be our focus in the following sections. Here, we concentrate on the integrator, as well as the necessary conversions between the simulator's components.

As in the physical experiment, the controller in our simulations receives sensor readings at a finite sampling frequency f_s (unspecified for now). The actuator forces are assumed to be applied instantaneously, and be held constant until the next sensor readings come in. Thus, both the strain readings and the actuator forces in our simulations need to be updated every $\Delta t = f_s^{-1}$ seconds.

The simulation, then, proceeds as follows. At time $t = 0$, the initial modal amplitudes $\{q\}_{init}$ are converted to strains (designated in the figure by a column vector $\{s\}$) and handed off to the controller. The controller comes back with the actuator forces, $\{f\}$, which are converted to the modal forces $\{u\}$. The integrator then uses both the initial modal state of the system, and the modal forces obtained, to determine the modal state of the system at time $t = \Delta t$. The new modal amplitudes are again converted to strains and given to the controller, and the process repeats. At

each step, the integrator uses the current modal state of the system and the modal forces supplied by the controller to determine the next modal state. The duration of the simulation, t_{sim}, as well as the initial modal state of the system, $\{q\}_{init}$ and $\{\dot{q}\}_{init}$, are specified by the user.

The integrator works by integrating, separately for each mode i, the modal equation of motion, (4.2). As mentioned earlier, equation (4.2) is a simple second-order linear ODE. With the modal force $u_i(t)$ held constant for the duration Δt of the integration, the solution to (4.2) can be expressed analytically in terms of the initial modal amplitude and velocity, q_i and $\dot{q}_i$. Thus, for each integration, the modal state at time $t + \Delta t$ is essentially directly calculated from the modal state at time t.

It remains to describe the conversions from modal amplitudes to strains, and from actuator forces to modal forces. In order to convert from $\{q\}$ to $\{s\}$, we first convert from $\{q\}$ to $\{y\}$, the nodal coordinates, by utilizing equation (4.7). With the beam displaced in the shape now described by $\{y\}$, we need to differentiate the displacement pattern twice to obtain the curvature, and thus the strains (see equation (3.27)). Although $\{y\}$ is not a continuous function that can be differentiated, it does describe such a function—namely, the cubic polynomial which is an approximation of the exact shape of the beam $y(x,t)$. We can thus still use equation (3.27) to calculate strain at particular points along the beam, given the nodal displacements $\{y\}$. The five points at which the strain is evaluated are the midpoints of the five beam elements, corresponding approximately to the locations of the sensors in the actual structure. The result of this evaluation is that the strain at any sensor i can be expressed purely in terms of the values of rotation angles θ_i and θ_{i+1} of the adjacent nodes:

$$s_i = \frac{a(\theta_i - \theta_{i+1})}{L/5} \tag{4.9}$$

(where a is the thickness of the beam, as before). We thus use the formula (4.9) to calculate the strains from the nodal displacements.

Finally, the conversion from actuator forces $\{f\}$ to modal forces $\{u\}$ is again broken up into two subproblems. First, the 10 nodal forces are calculated given the 5 actuator forces. Since the only forces our actuators are capable of applying are actually bending moments, all the entries in the force vector $\{U\}$ corresponding to the lateral forces are set to zero,

$$U_{y_i} = 0 \tag{4.10}$$

(there are 4 such entries, for nodes 2 through 5; the lateral forces at the end nodes are automatically zero because of the boundary conditions). The rest of the entries are filled in by calculating the bending moments applied at each of the nodes. Here, we refer to figure 2-6b. Since each node (other than the end nodes) is adjacent to two actuators, the bending moment applied at the node is the sum of the bending moments due to the forces applied by both of the adjacent actuators:

$$U_{\theta_i} = a(f_i - f_{i-1}) \tag{4.11}$$

For nodes 1 and 6, the bending moments applied are af_1 and $-af_5$, respectively. Finally, once we determine the nodal force vector $\{U\}$, we convert it to the vector of modal forces $\{u\}$ by applying equation (4.8).

Simulating Noise

In order to understand the effects of measurement noise on the controller's performance, we perform some simulations in which the strain readings are assumed to be noisy. To facilitate such experiments, included in the simulator is an optional "noisification" stage, in which the clean strain readings are made noisy before being passed on to the controller.

The noise function employed by the noisification procedure produces Gaussian "white" noise centered around the exact strain value. We will have more to say about the particular noise levels simulated when describing the results of these experiments.

4.1.4 Performing Optimization

In order to determine the optimal control gains of various controllers, we perform multidimensional optimization, as discussed in chapter 2. More precisely, the optimizer is essentially an implementation of the downhill simplex method, described in [28]. Given an initial set of gains and a merit function, this method strives to find a set of gains which minimize the value of the merit function (see figure 4-3). In our case, the merit function is implemented on top of the simulator, which utilizes some particular controller. When the gains are supplied to the merit function, they are passed on to the controller, and the simulation is then run for a pre-specified amount of time, t_{sim}. At every step in the simulation, the modal amplitudes and velocities, $\{q\}$ and $\{\dot{q}\}$, are recorded, such that at the end of the simulation we have the knowledge of the modal states for the entire run, $\bigcup_{t=0}^{t_{sim}} \{q\}_t$ and $\bigcup_{t=0}^{t_{sim}} \{\dot{q}\}_t$. The merit of the given set of gains is then evaluated based on the collected modal states.

Since the goal of any controller is to keep the deflection of the beam close to zero, our merit function has to penalize high deviations away from the equilibrium. It is also undesirable to have the beam swinging at high speeds; thus, high velocities have to be penalized as well. We take both of these concerns into account when evaluating the merit of a particular run. First, all the modal states $\{q\}$ and $\{\dot{q}\}$ are converted into their physical equivalents. (Actually, instead of computing the 10 nodal displacements and velocities, $\{y\}$ and $\{\dot{y}\}$, we calculate displacements $y_1, \ldots, y_5$ and velocities $\dot{y}_1, \ldots, \dot{y}_5$ at the 5 sensor locations.) We then calculate the following two values, v_1 and v_2:

$$v_1 = \sum_{t=0}^{t_{sim}} \sum_{i=1}^{5} y_i^2, \qquad v_2 = \sum_{t=0}^{t_{sim}} \sum_{i=1}^{5} \dot{y}_i^2$$

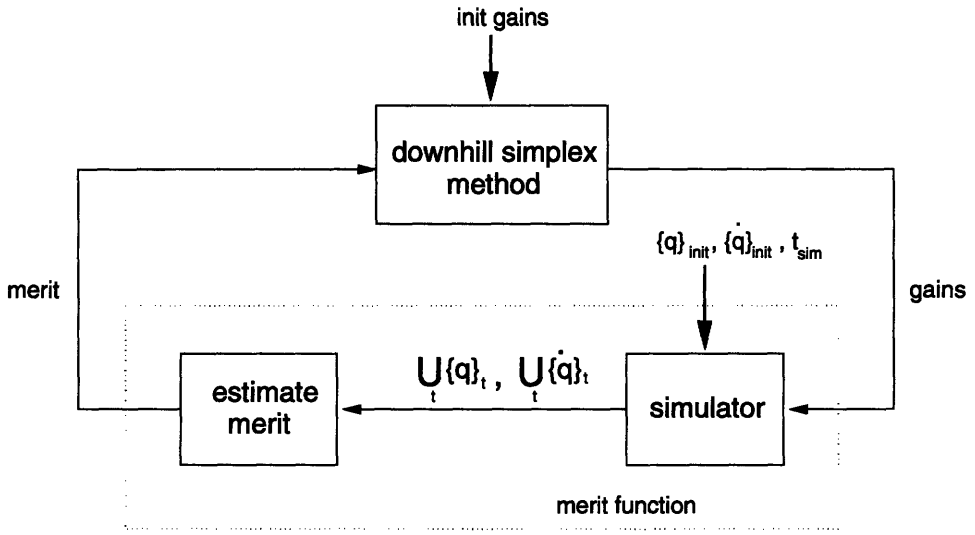

Figure 4-3: The flow of data through the optimizer. The optimizer works by running the downhill simplex algorithm to determine a set of gains which minimize the value of the merit function (an initial set of gains is provided by the user). The merit function used is implemented on top of the simulator; it uses the modal states, $\bigcup_{t=0}^{t_{sim}} \{q\}_t$ and $\bigcup_{t=0}^{t_{sim}} \{\dot{q}\}_t$, generated during a simulation to evaluate the merit of a given set of gains.

That is, v_1 is the sum of the squares of displacements at the 5 sensor locations taken for all time, and v_2 is the corresponding sum of the squares of velocities. Finally, the value returned by the merit function is the quantity $v_1 + kv_2$, for some constant scaling factor k. The scaling factor represents the relative importance of minimizing displacements vs. velocities of the vibrating beam. For the optimizations run as part of our experiments, k was selected and adjusted by hand, until the gains selected by the optimizer yielded beam behavior that was deemed reasonable.

4.2 Local Controller Implementation

Having familiarized ourselves with the workings of the simulator and the optimizer, we now use these tools to implement and evaluate control strategies. In this and the following sections, we take a look at the implementation of the local and modal controllers, respectively.

The implementation of the local controller is extremely straightforward. Essentially, we implement equation (3.29), which can be rewritten in vector form as follows:

$$\{f\} = P\{s\} + D\{\dot{s}\} \tag{4.12}$$

The strains $\{s\}$ are provided to us by the sensors, so all we have to do inside the control law is to keep track of the strain derivatives, $\{\dot{s}\}$. This is also straightforward; at any time t, the strain derivatives are computed from the sensor readings at times t and $t - \Delta t$, as follows:

$$\{\dot{s}\}_t = \frac{\{s\}_t - \{s\}_{t-\Delta t}}{\Delta t} \tag{4.13}$$

Thus, all that is required is for the controller to always keep a record of strains measured at the previous time step. The actuator forces can then be easily calculated from the current strains by applying equations (4.12) and (4.13). If any actuator force f_i happens to exceed the actuator limit, its value is simply cut off at the limit.

The beauty of local control is its simplicity, demonstrated convincingly by equations (4.12) and (4.13). Note that, although both of these are vector equations, the scalar equations they represent are completely independent of one another. Thus, for example, the actuator force f_1 applied by actuator 1 depends only on the strains measured by sensor 1. This, of course, is the reason for the name "local control."

4.3 Modal Controller Implementation

The modal controller is not nearly as easy to implement as the local one. Fundamentally, this is because the control law operates in modal space, while both sensing and actuation are performed in the physical space. The controller thus has to convert between physical and modal domains, much like we had to do in our simulator. The trouble, as we shall see shortly, is that the information contained in the sensor readings received by the controller is not sufficient to reconstruct the modal data exactly. In addition, the actuators are not always capable of applying the modal forces specified by the controller. We will investigate both of these effects in detail as we step through the modal control law implementation.

One consequence of having 5 discrete actuators is that our modal controller is only capable of controlling 5, rather than 10, modes of vibration. The intuition for this is that, since the relationship between modal and physical forces is linear, the number of forces we can specify in the modal domain must equal to the number of forces exerted in the physical domain; the details of this will become more clear in the discussion that follows. Since it is more important in buckling control to minimize vibrations of the low modes, we choose to control the lowest 5 modes and leave the higher modes uncontrolled. The uncontrolled modes of the system (here, modes 6 through 10) are often called its *residual modes.*

For the sake of clarity, we divide the control law implementation into three steps, as pictured in figure 4-4. First, the strain readings $\{s\}$ and their derivatives $\{\dot{s}\}$ are converted into $\{\hat{q}\}$ and $\{\hat{\dot{q}}\}$,[2] the estimates of the modal amplitudes and velocities, respectively. The desired modal forces, $\{u\}$, are then computed based on the estimated modal state. Finally, the actuator forces $\{f\}$ to be applied are determined based on the desired modal forces. We now describe each of these steps in detail.

[2]The "hat" notation is used to distinguish the estimated values from their exact counterparts.

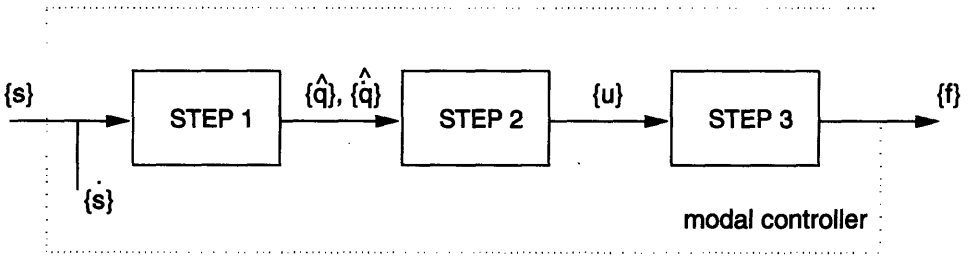

Figure 4-4: The 3 steps of the modal control law implementation. In the first step, the strain information, $\{s\}$ and $\{\dot{s}\}$, is converted into modal state estimates, $\{\hat{q}\}$ and $\{\dot{\hat{q}}\}$. The second step computes the modal forces $\{u\}$ based on the state information. The third and final step determines the actuator forces $\{f\}$ which correspond to the desired modal forces.

4.3.1 Step 1: Estimating Modal State

The first problem we are faced with is determining modal amplitudes and velocities based on the sensor readings. In particular, we have at our disposal the strains $\{s\}$ and the strain derivatives $\{\dot{s}\}$ (we can obtain the latter from the former, just as we did in the case of local control), and we would like to find $\{q\}$ and $\{\dot{q}\}$. Note, by the way, that since we only hope to control the 5 lowest modes of the system, those are the only modes we are actually interested in. We do not really care what the values are of modal amplitudes and velocities for the residual modes.

By analogy with the conversion process employed in our simulator, we would like to convert the strains $\{s\}$ to the modal amplitudes $\{q\}$ in two stages: by first converting strains to nodal displacements, $\{y\}$, and then carrying out the transformation $\{q\} = [C]^{-1}\{y\}$ (the inverse of the transformation given by equation (4.7)) from nodal to modal coordinates. It is clear, however, that the 5 strain values cannot be used to determine the entire nodal state $\{y\}$. For example, equation (4.9) indicates that the strains provide information only about the nodal angles θ_i, and not the nodal displacements y_i.

Taking a closer look at the transformations involved, we see from the relation $\{y\} = [C]\{q\}$ that each nodal angle θ_i is defined in terms of all 10 modal amplitudes, q_1 through q_{10}. If we now substitute θ_i and θ_{i+1} into equation (4.9) for each sensor i, we end up with a system of equations in which 5 strains $s_1, \ldots, s_5$ are expressed in terms of 10 modal amplitudes $q_1, \ldots, q_{10}$. This thought exercise makes it clear that the strains $\{s\}$ do not give us enough information to determine the modal amplitudes $\{q\}$.

How do we deal with this lack of information? A natural thing to try is to ignore the residual modes—i.e., to assume that the 5 highest modal amplitudes, q_6 through q_{10}, are so small that they can be approximated by zero. With 5 variables thus eliminated, we obtain a linear system of equations in which the strains $s_1, \ldots, s_5$ are expressed in terms of now only 5 (approximate) modal amplitudes, $\hat{q}_1, \ldots, \hat{q}_5$. This finally allows us to find the vector of modal amplitude estimates, $\{\hat{q}\} = [\hat{q}_1 \ldots \hat{q}_5]^T$, from the strains $\{s\}$. The vector of modal velocity estimates, $\{\dot{\hat{q}}\}$, is obtained in a completely analogous way from the strain derivatives $\{\dot{s}\}$.

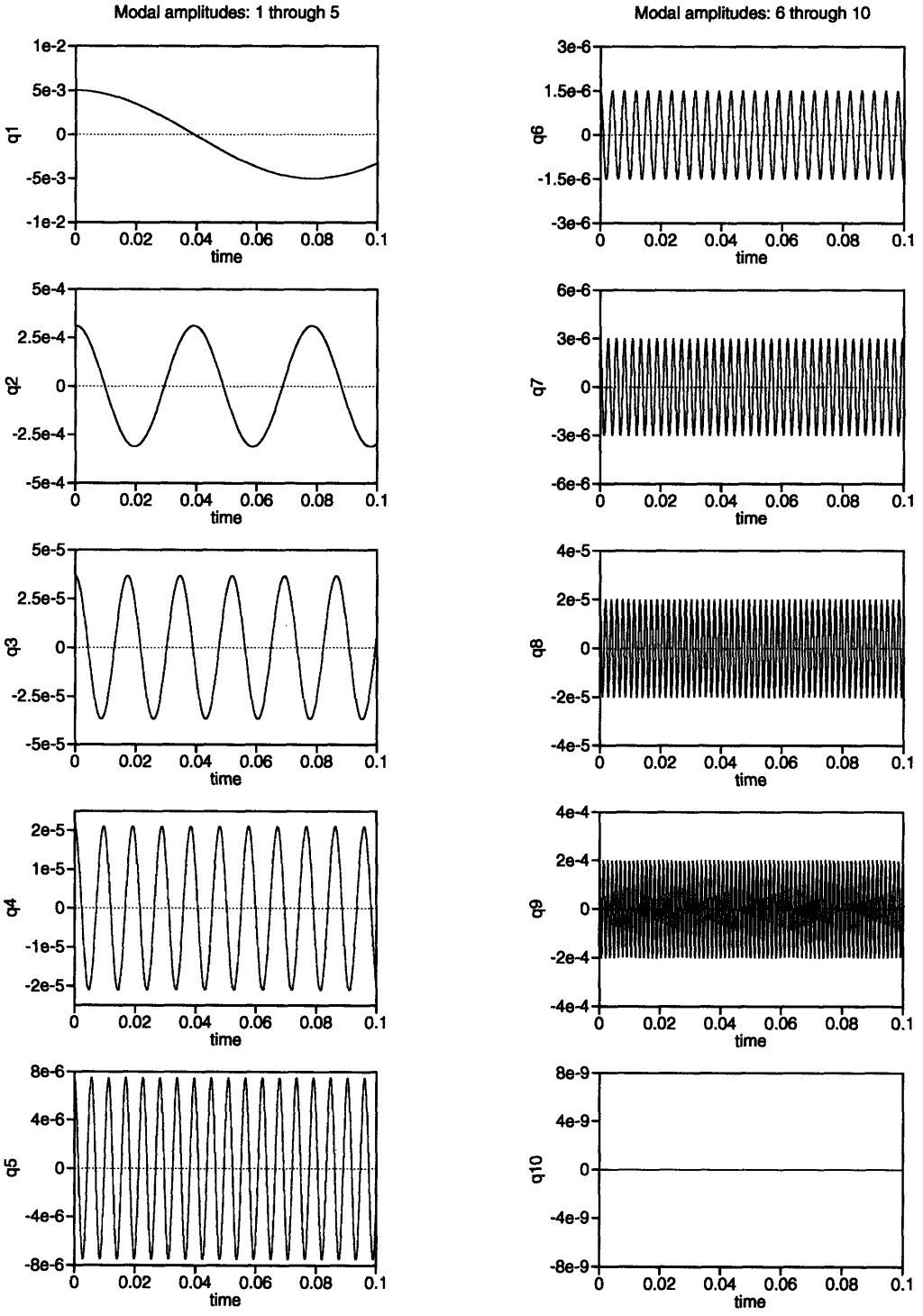

Figure 4-5: Modal amplitudes of the unloaded beam in free vibration. The initial modal state is as follows: $q_1 = 5.0 \times 10^{-3}$, $q_2 = 3.1 \times 10^{-4}$, $q_3 = 3.7 \times 10^{-5}$, $q_4 = 2.1 \times 10^{-5}$, $q_5 = 7.5 \times 10^{-6}$, $q_6 = 1.5 \times 10^{-6}$, $q_7 = 3.0 \times 10^{-6}$, $q_8 = 2.0 \times 10^{-5}$, $q_9 = 2.0 \times 10^{-4}$, $q_{10} = 1.0 \times 10^{-20}$, $\{\dot{q}\} = \{0\}$. The length of the simulation is $t_{sim} = 0.1$ seconds.

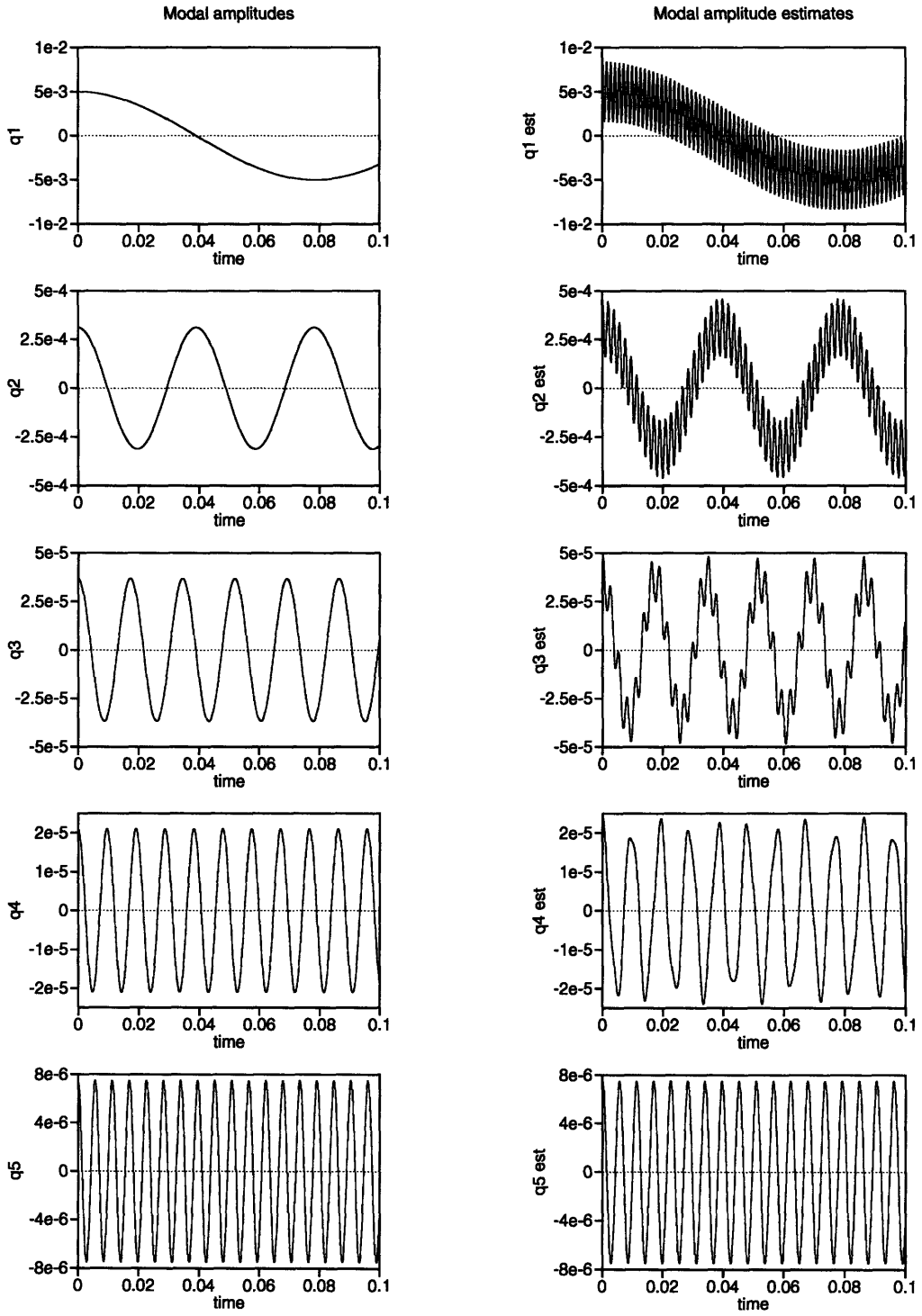

Figure 4-6: Modal amplitudes $q_1(t), \ldots, q_5(t)$ vs. amplitude estimates $\hat{q}_1(t), \ldots, \hat{q}_5(t)$ of the unloaded beam in free vibration. The estimates are obtained by assuming that the amplitudes of the residual modes are zero. The simulation parameters are as specified in figure 4-5.

Unfortunately, the approximation made in the previous paragraph—that the amplitudes and the velocities of the residual modes can be approximated as zero—is not a very good one. For example, we will see later on in this section that, because not all desired modal forces are realizable given the actuators at hand, the modal controller itself is responsible for continuously exciting the residual modes. Thus, by ignoring the residual modes, we introduce a rather significant error in the modal state estimates of the controlled modes. This phenomenon is known as *observation spillover* ([2], [3]).

The effects of observation spillover are demonstrated pictorially in figures 4-5 and 4-6. In this example, the beam is unloaded and uncontrolled. Instead of a controller, the simulation includes an *observer* which simply calculates and records the modal state estimates $\{\hat{q}\}$ and $\{\hat{\dot{q}}\}$ over the entire run, according to the scheme specified above. The initial modal state is picked based on average modal values observed in a typical experimental run. Because our simulator assumes no damping, each mode simply oscillates at its own modal frequency for the duration of the run, $t_{sim} = 0.1$ seconds. Figure 4-5 shows the resultant exact modal amplitudes $q_1(t), \ldots, q_{10}(t)$, and figure 4-6 compares the first five of these, $q_1(t), \ldots, q_5(t)$, to the modal amplitude estimates $\hat{q}_1(t), \ldots, \hat{q}_5(t)$ (modal velocities behave in a similar fashion).

Comparing the plots of $q_1(t), \ldots, q_5(t)$ and $\hat{q}_1(t), \ldots, \hat{q}_5(t)$ in figure 4-6, we see that the amplitude estimates produced by assuming zero residual mode amplitudes contain high frequency components. In effect, the residual modes "spill over" into our estimates of the controlled mode values. For example, the modal amplitude estimate $\hat{q}_1$ in figure 4-6 has a high frequency component which looks like the modal amplitude q_9 of figure 4-5. This suggests that given only 5 sensor readings, $s_1, \ldots, s_5$, the controller cannot distinguish between modes 1 and 9; it thus attributes vibrations in mode 9 to mode 1. Indeed, this aliasing between modes 1 and 9 can be seen from figure 4-7, which shows the sensor locations on the beam relative to the mode shapes $\psi_1(x)$ and $\psi_9(x)$.

It can be verified that just as mode 9 aliases into mode 1 via observation spillover, the same is also true for modes 8 and 2, 7 and 3, and 6 and 4. This can also be seen by comparing the plots of figures 4-5 and 4-6. Mode 10, on the other hand, does not spill into any other mode, as the sensors cannot even see it: the locations of all 5 sensors correspond to the zeroes of the mode shape $\psi_{10}(x)$.

Because the modal controller uses the aliased modal estimates to compute the control forces, observation spillover greatly affects the system's ability to support

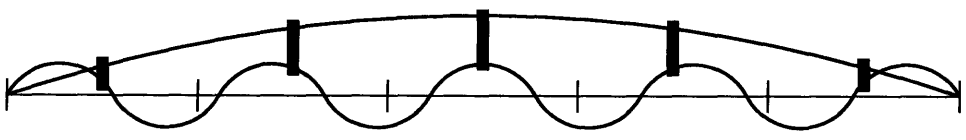

Figure 4-7: Aliasing between modes 1 and 9. The beam is broken up into 5 elements; each black rectangle indicates the sensor location in the middle of the corresponding element. With this placement of the sensors, the control system cannot differentiate between the mode shapes $\psi_1(x)$ and $\psi_9(x)$.

large compressive loads. We shall explore the effect of observation spillover on system performance in section 4.4.

4.3.2 Step 2: Calculating Modal Control Forces

Once the modal state estimates have been obtained, it is straightforward to calculate the modal forces, based on the gains of the control law. Given the gains P_i, D_i for each controlled mode $i = 1, \ldots, 5$, the corresponding modal force u_i is essentially determined from equation (3.26). In it, we replace the exact modal amplitudes q_i and $\dot{q}_i$ by their estimates:

$$u_i = P_i \hat{q}_i + D_i \hat{\dot{q}}_i$$

For the residual modes, we would like the modal forces $u_6, \ldots, u_{10}$ to be zero, since non-zero forces would cause unwanted high mode excitations. Combining the modal forces for the controlled and the residual modes, we thus obtain the 10-element modal force vector $\{u\}$.

4.3.3 Step 3: Determining Actuator Forces

In the final step of modal controller implementation, we are faced with determining the actuator forces corresponding to the desired modal control forces. In order to obtain a relationship between the modal forces $\{u\}$ and the actuator forces $\{f\}$, we substitute equations (4.10) and (4.11) into equation (4.8). Since each U_{θ_i} is a linear combination of the actuator forces, and all the lateral forces U_{y_i} are zero, we obtain a linear system of equations in which the 10 modal forces $u_1, \ldots, u_{10}$ are expressed in terms of the 5 actuator forces $f_1, \ldots, f_5$. Therefore, all of the actuator forces are uniquely determined by any 5 of the 10 modal forces: once we specify 5 values for the elements of $\{u\}$, the actuator forces $\{f\}$, as well as the remaining 5 elements of $\{u\}$, are automatically decided. What this means is that not every modal force vector $\{u\}$ is physically realizable—i.e., the actuators are not always capable of applying the exact modal forces specified by the controller.

How do we then go about realizing an unrealizable set of modal control forces? As in step 1, the natural solution is to sacrifice the residual modes in favor of the controlled ones. Specifically, we can determine the actuator forces to be applied by setting the modal forces for the 5 controlled modes to their desired values $u_1, \ldots, u_5$. This automatically determines the residual mode forces $u_6, \ldots, u_{10}$, which turn out to be non-zero in general. As a result, the actuator forces calculated in this manner do not only apply the desired controlled mode forces, but also act to excite the residual modes, a phenomenon known as *control spillover* ([2], [3]).

Control spillover is similar to observation spillover in a sense that it involves aliasing between the controlled and the residual modes. For example, just like the sensors cannot distinguish between modes 1 and 9, the actuators cannot apply a force to mode 1 without also applying a force to mode 9. Similarly, the modal forces for

modes 2, 3, and 4 spill into the forces for modes 8, 7, and 6, respectively. We will witness this phenomenon in section 4.4, when examining the behavior of the simulated beam under modal control.

Actuator Limits

So far, in the process of determining actuator forces, we have not concerned ourselves with the actuator limits. What do we do if one or more of the actuator forces computed above exceeds the maximum force the actuators are capable of applying? The most obvious answer is to simply cut off the actuator force at the limit, or saturate it. However, saturating the actuator forces could change the corresponding modal control forces in an undesirable way. For example, through saturation, we could reduce u_1 while keeping u_5 the same, even though we know that it is more important, in buckling control, to stabilize mode 1 than mode 5. In general, saturating the actuator forces implies decreasing some of the modal force values, and increasing others; we have no explicit control over which of the modal forces get reduced. Furthermore, saturation may cause additional control spillover into high frequency modes.

Ideally, we would like to limit the control forces in the modal, rather than the physical, domain. This would give us the freedom to reduce the modal forces for the higher (i.e., less important) modes before the ones for the lower modes. Thus, faced with the problem of limiting the actuator forces, we would start by reducing u_5, the desired modal force for mode 5; if that were not good enough, we would proceed to reduce u_4; and so on.

In fact, that is exactly how our controller deals with actuator forces that exceed the actuator limit. It first computes the actuator forces corresponding to the desired modal forces $u_1, \ldots, u_5$, as described previously. If any of the resultant actuator forces exceed the limit, then u_5 is set to zero, and the actuator forces are recomputed; if any of these exceed the limit, u_4 is set to zero, and the actuator forces are recomputed again; and so on. Once we obtain a set of actuator forces which are all under the limit, we go back and add in fractions of those modal forces which have been cut off that just keep the actuator forces under the limit. For example, suppose we had to set u_5 to zero in order to obtain an actuator force vector $\{f\}$ with all its entries smaller than the actuator limit; then, we would determine a new u_5 greater than zero (but smaller than the original u_5, of course) that would keep the corresponding actuator forces just under the limit; finally, these actuator forces would be the ones applied to the beam.

4.4 Simulation Results

In this section, we use the machinery described above to simulate the behavior of the beam under both modal and local control, and compare the results. Our primary goal is to investigate the potential of both controllers to increase the load-bearing strength of the beam, and to understand the reasons for their limitations.

Of course, the amount of weight the beam is capable of supporting depends not

only on the control law being used, but on many other properties of the control system, as well as the beam itself. For example, the geometry and the material properties of the beam have a major effect on the beam dynamics, as demonstrated by equation (3.19). Other important parameters include the strength of the actuators used to exert the control forces, the sampling frequency f_s of the controller, and the amount of measurement noise present in the system. Finally, it is important to know the magnitude of a typical disturbance to the system. The larger the disturbance, the higher the control forces needed to push the beam back to its equilibrium position; with only a limited amount of control authority available, larger disturbances translate into smaller sustainable axial loads.

In our simulations, we pick the above parameters so as to approximate the real system as closely as possible. In particular, the geometry of the simulated beam matches that of the prototype beam (see section 2.1.1); however, because of the assumption of uniformity, the effects of the sensors and actuators on the material properties of the beam are neglected in simulation. The actuator strength is taken to be equal to the strength of the piezo-ceramic actuators employed in the real system (see section 2.1.3). The sampling frequency of the controller, $f_s = 3.8$ kHz, is also taken to match the frequency of the real controller.[3] As for the noise levels, we assume no measurement noise for now; we shall investigate the effects of noise on the system later on in this section.

In order to simulate the system subjected to a disturbance, we start the simulation with the beam away from its equilibrium position. The initial modal amplitude and velocity vectors, $\{q\}_{init}$ and $\{\dot{q}\}_{init}$, are picked to match the typical modal values observed in the experimental runs on the prototype beam:

$$\{q\}_{init} = \begin{bmatrix} 5.0 \times 10^{-3} \\ 3.1 \times 10^{-4} \\ 3.7 \times 10^{-5} \\ 2.1 \times 10^{-5} \\ 7.5 \times 10^{-6} \\ 0 \\ \vdots \\ 0 \end{bmatrix}, \qquad \{\dot{q}\}_{init} = \{0\} \tag{4.14}$$

The amplitudes are specified in units of meters; for example, the first mode has amplitude 5 mm. Modal amplitudes decrease with the mode number, as expected; the residual modes are assumed to have zero initial amplitude. The modal velocities of all 10 modes are assumed to be zero as well.

With simulation parameters specified as above, we now subject the beam to a compressive load, and simulate the behavior of the beam under both modal and local control. The control gains for each of the two controllers are obtained via numerical

[3] At the end of the section, however, we will present simulation results for controllers operating at a wide range of sampling frequencies.

optimization, as described earlier in this chapter. The amount of compressive load applied to the beam is increased until a value is reached for which the controller fails to stabilize the beam. Below, we present the results of these simulations for the cases of modal and local control, in turn.

4.4.1 Modal Control

Under modal control, the value of the maximum compressive load supported by the beam in simulation is approximately 6.2 Newtons. The buckling load for the simulated beam turns out to be about 1.5 Newtons; this implies a factor of 4.1 increase in the load-bearing strength of the beam.

Figure 4-8 shows the modal amplitudes $q_1, \ldots, q_{10}$ of the beam subjected to the maximum sustainable load over a 2 second run. The controlled modes—modes 1 through 5—are shown in the left column, while the residual modes—modes 6 through 10—are plotted on the right. It is clear from the figure that the beam is eventually stabilized in its equilibrium position; even after 2 seconds, most of the modes have their amplitudes reduced very close to zero.

Taking a closer look at the plots of figure 4-8, we notice, first of all, that the residual modes (with the exception of mode 10) have non-zero modal amplitudes throughout the run, in spite of zero amplitudes at time $t = 0$. Furthermore, the residual modes do not simply oscillate at their respective frequencies of vibration; instead, they are composed of both high frequency and low frequency components. For example, the response of mode 9 is a superposition of a low frequency component, which looks similar to the negative of mode 1, and a high frequency component, corresponding to the vibrations at the natural frequency of mode 9.

This phenomenon illustrates the effect of control spillover. The modal force $u_1(t)$ applied to mode 1 is approximately proportional to the negative of the modal amplitude, $q_1(t)$. Because of control spillover, $u_1(t)$ aliases into the modal force $u_9(t)$ for mode 9, so $u_9(t)$ also ends up having a low frequency component approximately proportional to $-q_1(t)$. Since the frequency of mode 1 is much smaller than the natural frequency of mode 9, this low frequency component of $u_9(t)$ looks essentially like a quasistatic force to mode 9. As a consequence, the modal amplitude $q_9(t)$ has a low frequency component that follows the modal force $u_9(t)$, and is thus approximately proportional to $-q_1(t)$. In addition, $q_9(t)$ has a high frequency component corresponding to the natural frequency of mode 9, also excited by control spillover from mode 1.

Figure 4-8 shows the effects of control spillover on the rest of the residual modes as well. Thus, the low frequency component of mode 8 looks like a scaled down and inverted version of mode 2; in this case, the high frequency oscillations at the natural frequency of mode 8 are only visible at the beginning of the run, and decay to zero within a short period of time. Similarly, modes 7 and 6 look like modes 3 and 4, respectively; the high frequency components of modes 7 and 6 (not visible in the plots of figure 4-8) also decay to zero soon after the start of the simulation.

While control spillover acts to excite the residual modes, it does not by itself have an effect on the behavior of the controlled modes. However, the controlled modes *are*

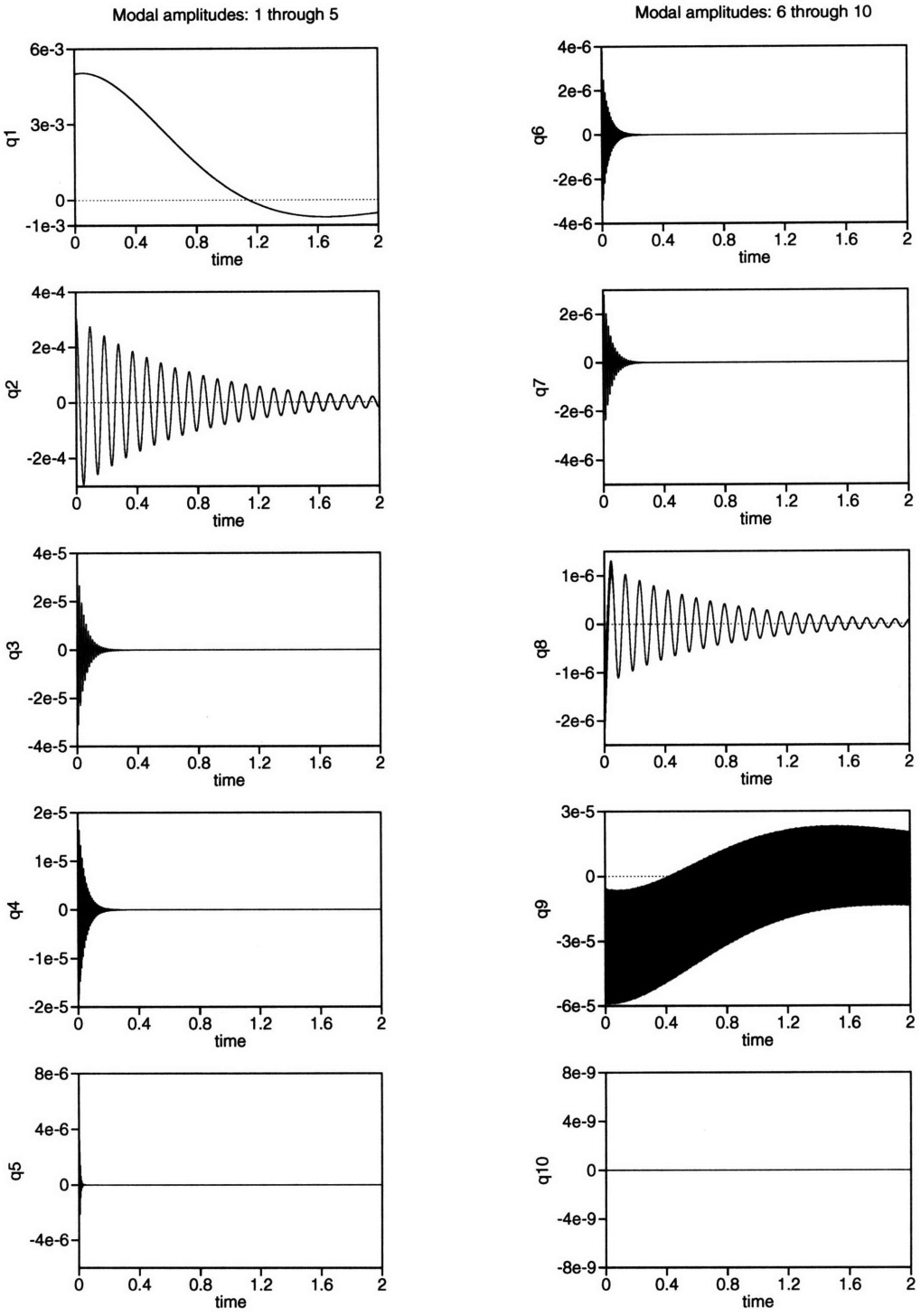

Figure 4-8: Modal amplitudes of the simulated beam under modal control. The compressive load used is equal to the maximum sustainable load of 6.2 Newtons, or 4.1 times the buckling load. The sampling frequency used by the controller is 3.8 kHz. The initial state of the beam is given by equation (4.14). The length of the simulation is $t_{sim} = 2$ seconds.

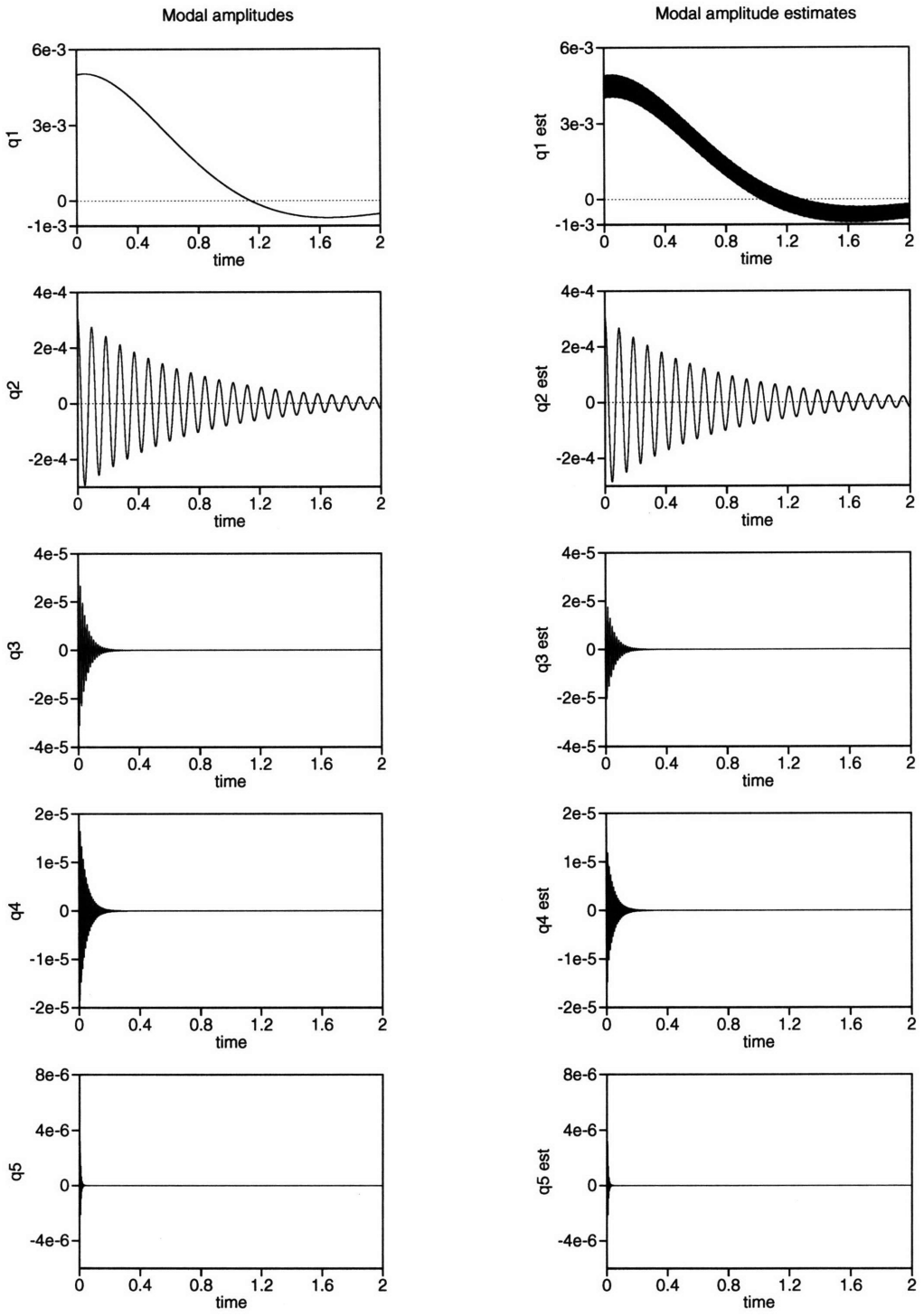

Figure 4-9: Modal amplitudes $q_1(t), \ldots, q_5(t)$ vs. modal amplitude estimates $\hat{q}_1(t), \ldots, \hat{q}_5(t)$ of the simulated beam under modal control. The simulation parameters are as specified in figure 4-8.

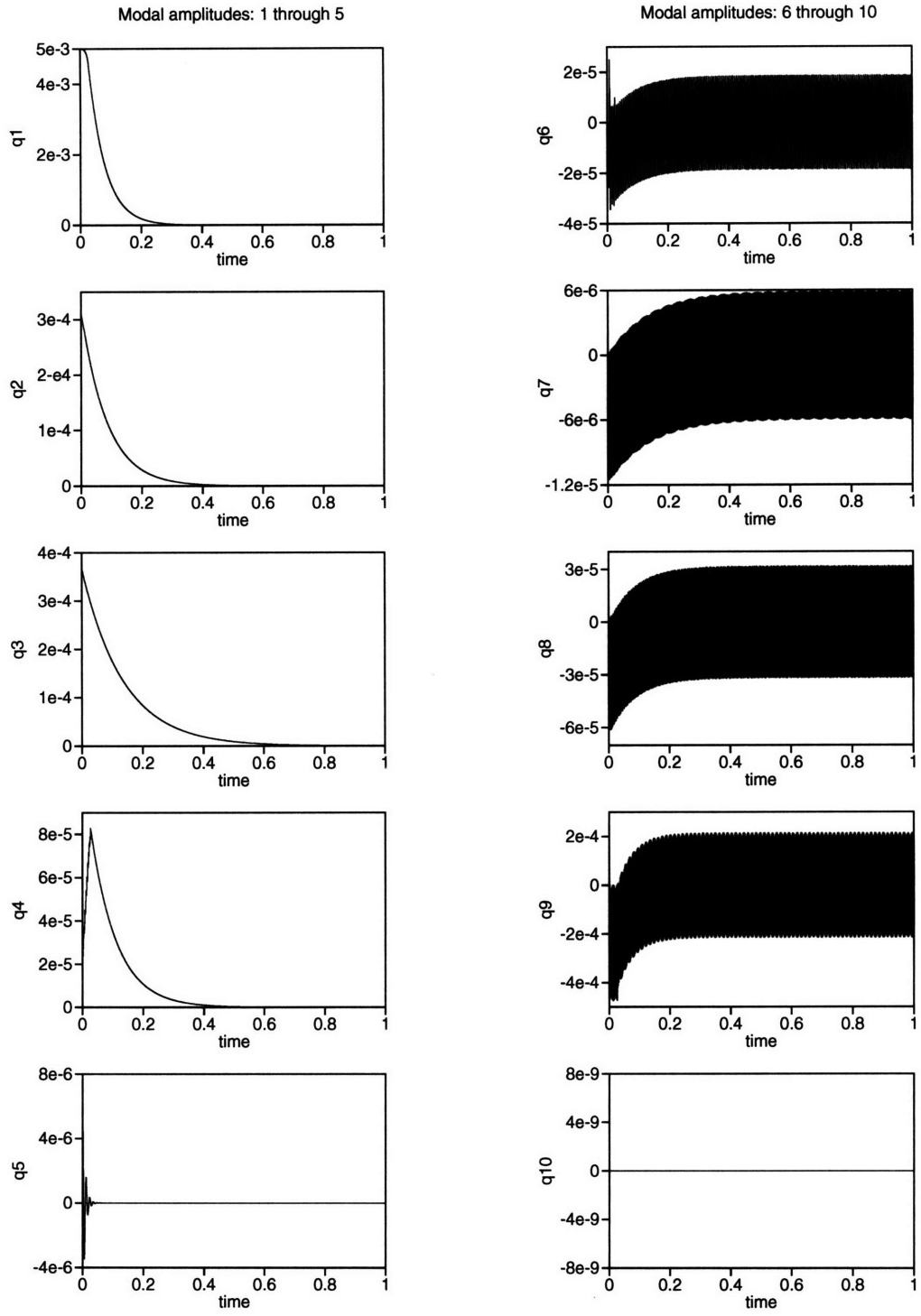

Figure 4-10: Modal amplitudes of the simulated beam under idealized modal control. The idealized controller uses the exact modal amplitudes $q_1(t), \ldots, q_5(t)$, rather than the estimates $\hat{q}_1(t), \ldots, \hat{q}_5(t)$, to control the beam. The compressive load used in this run is the maximum sustainable load of 29.1 Newtons, or 19.2 times the buckling load. The sampling frequency used by the controller is 3.8 kHz. The initial state of the beam is given by equation (4.14). The length of the simulation is $t_{sim} = 1$ second.

affected by observation spillover. This is apparent from figure 4-9, which compares the exact modal amplitudes of the first five modes (left column) to their estimates $\hat{q}_1(t), \ldots, \hat{q}_5(t)$ obtained by the controller (right column). For example, because the controller cannot distinguish mode 1 from mode 9, the modal estimate for mode 1 is a weighted sum of the modal amplitudes for modes 1 and 9 ($q_1(t)$ and $q_9(t)$ from figure 4-8). The effect of observation spillover on the rest of the controlled modes is not as evident from the figure, as the amplitudes of modes 6, 7, and 8 are not large enough to be visible.

Because the controller uses the aliased modal amplitude estimates to compute the control forces, observation spillover has serious implications for system performance. For example, it is clear from figure 4-9 that the modal force $u_1(t)$ applied by the controller has a high frequency component, corresponding to the high frequency component present in the modal estimate $\hat{q}_1(t)$. The amplitude of this component must not be too large, so as to keep mode 1 from becoming unstable. This means that the amplitude of mode 9 must be small, or that the control spillover from mode 1 into mode 9 must be kept low. Thus, the control authority dedicated to mode 1 cannot be too large. This condition imposes a serious limitation on the maximum compressive load sustainable by the system.

To further investigate the effects of observation spillover on system performance, we implement an idealized version of the modal controller in which the real modal amplitudes, $q_1(t), \ldots, q_5(t)$, rather than the modal estimates, are used to control the beam. This idealized system performs significantly better: the maximum load supported by the beam is 29.1 Newtons, or 19.2 times the buckling load—a factor of 4.7 higher than the value achieved by the modal controller!

The modal amplitudes obtained by running the idealized modal controller on the beam subjected to the maximum sustainable load are shown in figure 4-10. The residual modes in figure 4-10 still exhibit the effects of control spillover: they are composed of both high frequency and low frequency components. However, due to the absence of observation spillover, the controlled modes are not affected by the high frequency excitations, and are stabilized quickly and effectively.

Note in figure 4-10 that because the residual mode excitations do not interfere with the controlled modes, high frequency components of the residual modes do not decay to zero overtime: the residual modes are in fact uncontrolled. In contrast, the real modal controller is forced to control the residual modes of the system in addition to the controlled modes, in an effort to minimize observation spillover. Thus, the residual modes in figure 4-8 decay to zero overtime.

Controlling the residual modes is difficult if the sampling frequency of the controller is not significantly higher than the natural frequencies of the residual modes. For example, it turns out that for the simulated beam, the natural frequency of mode 9 is approximately equal to 700 Hz—only a factor of 5 or so smaller than the sampling rate of 3.8 kHz. A controller this slow finds it difficult to keep up with mode 9. As the sampling frequency of the controller is increased, we expect the modal controller to perform better. We shall investigate the effect of the sampling rate on controller performance later on in this section.

4.4.2 Local Control

The local controller in simulation performs almost as well as the modal controller: under local control, the beam is able to support a maximum axial load of approximately 6.1 Newtons, or 4.0 times the buckling load. The modal amplitudes of the beam subjected to this maximum load for the duration of 1 second are shown in figure 4-11. As before, the left column contains the controlled modes, while the right column shows the residual modes.

Comparing figures 4-8 and 4-11, we see that the modal response of the system under local control has the same character as the response under modal control. As before, each of the residual modes has both a low frequency and a high frequency component. Furthermore, like the modal controller, the local controller acts to stabilize the residual modes in addition to the controlled modes. These observations indicate that just like modal control, local control suffers from both observation and control spillover. The fundamental reason for this is that the strain data used as the basis for local control contains components of different frequencies, corresponding in the modal domain to vibrations in different modes. When the local controller acts on the strain readings, it excites all of those frequencies at once; in the modal domain, this results in control spillover. When the local controller reads the sensor data, it again sees the superposition of components of different frequencies; in the modal domain, this can be interpreted as observation spillover. The net effect is that the local controller behaves much like the modal controller, in spite of the differences in implementation.

4.4.3 Varying the Sampling Frequency

In order to investigate the effect of the sampling rate of the controller on the system performance, we run a series of simulations in which the maximum sustainable load is determined for a wide range of sampling frequencies. The results of these simulations are summarized in figure 4-12 and table 4.1.

Figure 4-12 plots the maximum load supported by the beam with respect to the sampling rate, for three types of controllers: modal, local, and idealized modal. (The idealized modal controller performs modal control in the absence of observation spillover; see figure 4-10.) Table 4.1 contains the numerical data corresponding to the data points of figure 4-12. The maximum sustainable load for various sampling frequencies is listed in the table both in units of Newtons, and as a ratio to the buckling load of the simulated beam. Idealized modal control is not included in the table; the maximum load supported via idealized control is 29.1 Newtons, or 19.2 times the buckling load, over the entire tested range of sampling frequencies.

As expected, the maximum sustainable load increases with the sampling rate for both modal and local control: higher sampling frequencies make it easier for the controller to control the residual modes. In contrast, the maximum sustainable load for idealized modal control stays constant over the entire sampling frequency range. This also makes sense, as the idealized controller does not suffer from observation

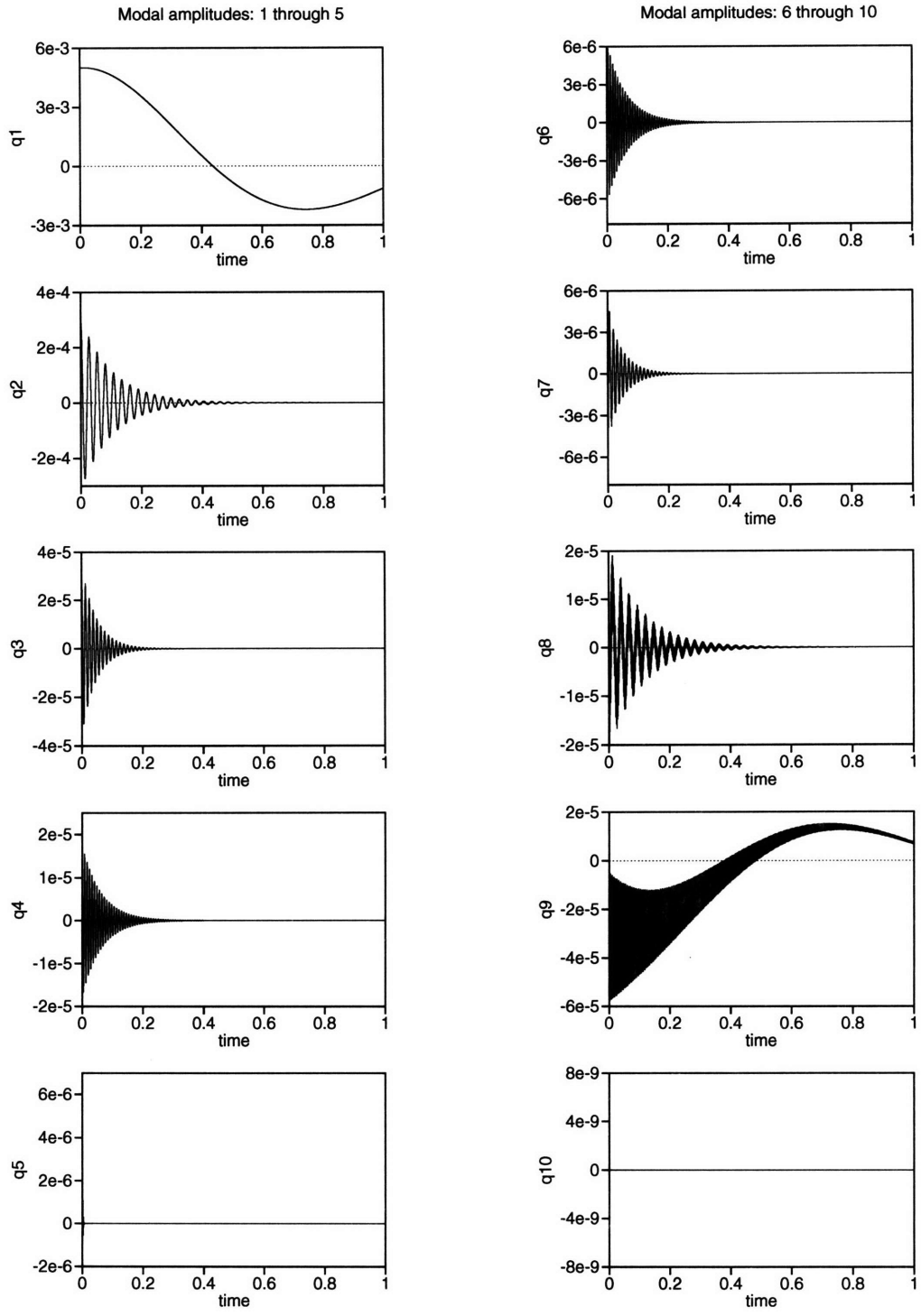

Figure 4-11: Modal amplitudes of the simulated beam under local control. The compressive load used is the maximum sustainable load of approximately 6.1 Newtons, or 4.0 times the buckling load. The sampling frequency used by the controller is 3.8 kHz. The initial state of the beam is given by equation (4.14). The length of the simulation is $t_{sim} = 1$ second.

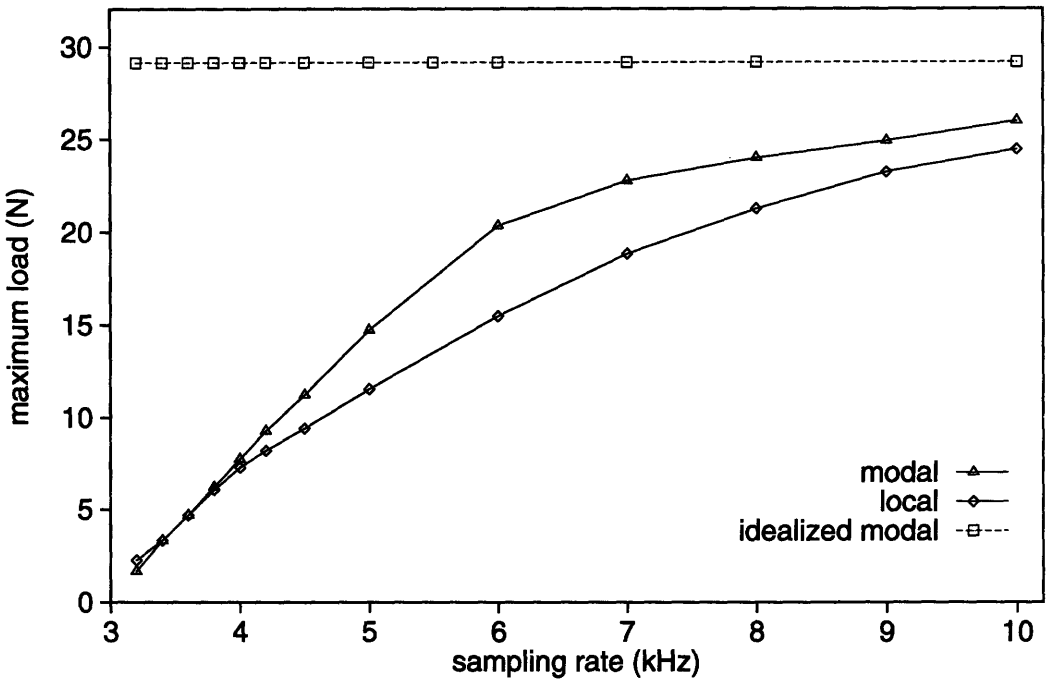

Figure 4-12: Maximum load supported by the beam (in Newtons) with respect to the sampling rate of the controller (in kHz), for three types of controllers: modal, local, and idealized modal. The buckling load for the simulated beam is approximately 1.5 Newtons.

sampling rate (kHz)	modal control		local control	
	max load (Newtons)	ratio to buckling load	max load (Newtons)	ratio to buckling load
3.2	1.67	1.1	2.28	1.5
3.4	3.34	2.2	3.34	2.2
3.6	4.71	3.1	4.71	3.1
3.8	6.22	4.1	6.07	4.0
4.0	7.74	5.1	7.29	4.8
4.2	9.26	6.1	8.20	5.4
4.5	11.23	7.4	9.41	6.2
5.0	14.73	9.7	11.54	7.6
5.5	18.07	11.9	13.66	9.0
6.0	20.34	13.4	15.49	10.2
7.0	22.77	15.0	18.83	12.4
8.0	23.99	15.8	21.25	14.0
9.0	24.90	16.4	23.23	15.3
10.0	25.96	17.1	24.44	16.1

Table 4.1: Tabulated data corresponding to the data points of figure 4-12. Maximum sustainable load for modal and local control is specified both in Newtons, and as a ratio to the buckling load of the simulated beam.

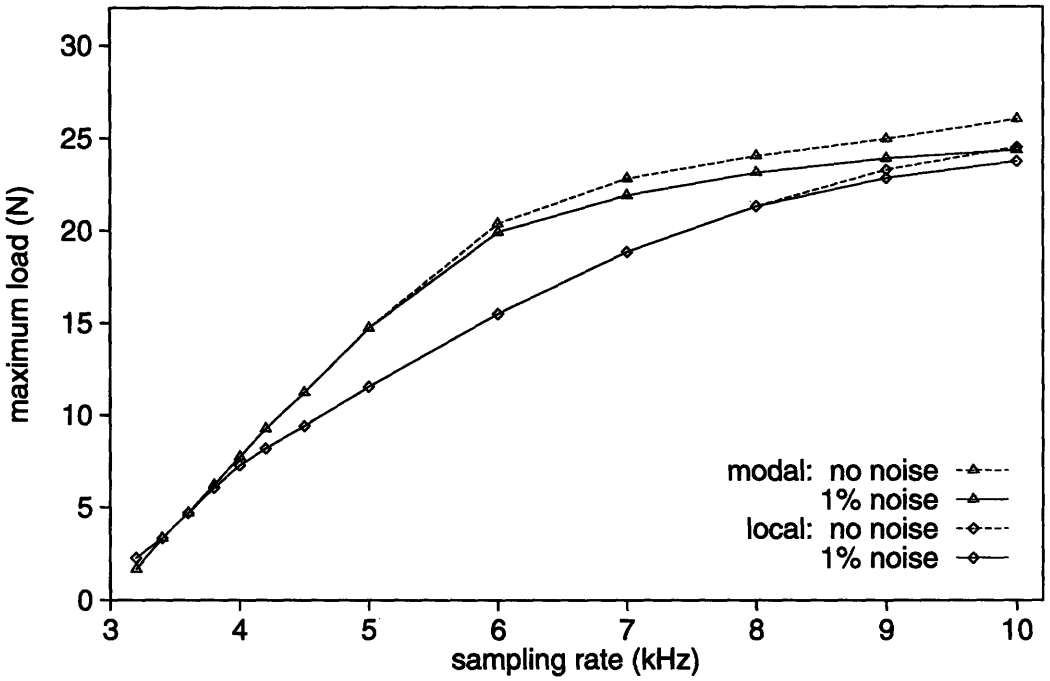

Figure 4-13: Effects of measurement noise on the maximum sustainable load. Maximum load supported by the beam (in Newtons) is shown with respect to the sampling rate of the controller (in kHz), for the modal and local controllers operating with and without measurement noise. The buckling load for the simulated beam is approximately 1.5 Newtons.

spillover, and thus only has to control the five low frequency modes of the beam.[4] Note also that the modal control curve in figure 4-12 approaches the asymptote provided by the idealized modal control curve: at higher sampling frequencies, the effect of observation spillover becomes less and less significant.

Figure 4-12 and table 4.1 also demonstrate that the local controller does not perform significantly worse than the modal controller no matter what sampling frequency is used by the control law. The local controller actually does slightly better at low frequencies, but is outperformed at frequencies higher than 3.6 kHz.

4.4.4 Effects of Noise

Figure 4-13 demonstrates the effects of measurement noise on system performance. The noise level chosen for the simulations is 1% of the initial strain value of the middle strain gauge. (Since the strain values of the successfully controlled beam decrease over time, this represents the maximum strain value sensed over the length of the run.) Figure 4-13 shows the maximum sustainable load with respect to the sampling rate of the controller, for the system with and without measurement noise.

The results in figure 4-13 are encouraging: neither of the two controllers suffers

[4]Of course, as the sampling frequency of the controller is reduced further, the idealized modal control curve eventually drops down, as the controller finds it difficult to keep up even with the low frequency modes.

a significant drop in performance as a result of measurement noise. At low sampling frequencies (and thus low sustainable loads), both controllers can tolerate noisy measurements without any effect on performance. As the maximum sustainable load increases with higher sampling frequencies, both controllers start experiencing difficulties maintaining the same levels of performance in the presence of noise. However, the decrease in the maximum sustainable load is rather small in all cases.

4.5 Concluding Remarks on Observation Spillover

As demonstrated by figures 4-12 and 4-13 above, both modal and local controllers can achieve impressive levels of performance—at least in simulation. However, the simulation results also indicate that one of the major factors limiting the performance of both controllers is the phenomenon of observation spillover. Unfortunately, observation spillover is an unavoidable problem in any control system with a finite number of sensors. Therefore, one important question that remains to be answered is whether we can reduce observation spillover, thereby improving the performance of the buckling controllers even further.

In [3], Balas discusses several possible ways to reduce the spillover problem. The most obvious of these involve redesigning the structure and/or relocating the control devices. For example, observation spillover can be reduced by increasing the number of sensors, or by relocating the sensors to be close to the zeros of the residual mode shapes. However, none of these solutions are applicable given the fixed design at hand.

The most promising method of reducing observation spillover in our system is filtering the sensor data in order to eliminate the unwanted high frequency components. In [2] and [3], Balas describes a "comb" filter that can be used to counteract spillover in systems concerned with control of vibration. The "teeth" of the comb are narrow bandpass filters; Balas proposes to implement them with phase-locked-loops (PLLs), tuned to the controlled frequencies. Besides its narrow-bandpass characteristic, the PLL has the advantage that it can lock onto the exact controlled frequency even if the frequency it is pretuned to is only approximately correct.

Instead of a comb filter, we experimented with a lowpass filter—specifically, a digital Butterworth filter of order 6 ([20], [24]).[5] The plots of magnitude and phase response of the filter are shown in figure 4-14. The cutoff frequency of the filter is chosen such that its value is between the controlled frequency of mode 5 and the (uncontrolled) frequency of mode 6 (this value varies for different axial loads, since modal frequencies depend on the load); thus, the residual modes are filtered out, while the controlled modes are passed through. The filter is applied to each of the sensor readings $s_i(t)$, thereby producing strain values with no high frequency components. The resultant strains are then used by the controllers as before: the local controller uses the strains directly, while the modal controller first converts them to modal state

[5]The filter was designed using Matlab ([21]). Once the filter coefficients were generated by Matlab, they were incorporated into the controller.

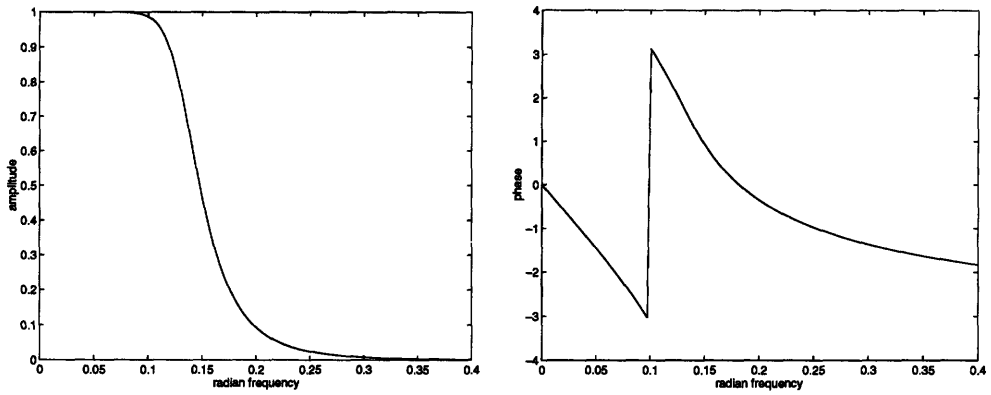

Figure 4-14: Magnitude and phase response of an order 6 digital Butterworth filter. The magnitude response is shown on the left, while the phase response is on the right. The radian frequency is given by ωT_s, where ω is the signal frequency is radians, and $T_s = \frac{1}{f_s}$ is the sampling period. The particular cutoff frequency of the filter is not important here, as it differs depending on the axial load.

estimates.

Unfortunately, the process of filtering the strain data has one undesirable side effect—namely, it introduces phase delay. This is explained by the phase response of the filter, shown in figure 4-14. Phase distortion is common to all lowpass filters. In typical filter applications, such as communications, non-zero phase response is usually deemed acceptable; the ideal is considered to be *linear phase* response ([24], [20]), which guarantees that all frequency components of the input signal are delayed by the same amount—i.e., the shape of the signal is preserved. In a control system, however, phase distortion presents a serious problem. With the state estimates out of phase with the exact state, the controller calculates control forces based on outdated state information; the results could be disastrous if the phase delay is significant.

Indeed, because of phase distortion, the filter described above fails to improve the performance of the simulated buckling control system. Although most of the observation spillover is successfully eliminated, the phase delay introduced by the filter renders the system unstable, at loads even smaller than those achieved in the presence of observation spillover.

We do not attempt to counteract the effects of phase distortion on system performance as part of the work described in this thesis. Perhaps with proper care, however, phase distortion can be made less severe, or compensated for in some way (e.g., with more sophisticated filtering techniques). This remains a subject of possible future research.

Chapter 5

Experimentation

In chapters 3 and 4 we investigated the behavior of the modal and local controllers by means of qualitative analysis and simulation, respectively. We now present the results of experiments performed on the prototype beam described in chapter 2, and discuss the discrepancies between the experimental results and the results of analysis and simulation obtained previously.

5.1 Experimental Results

In the experiments performed on the prototype column, the uncontrolled beam is initially subjected to a given axial load, and positioned by hand to be approximately in its equilibrium (straight) position. The controller (either modal or local) is then turned on, and the beam is released. An initial reading of the sensors is taken by the controller to indicate the desired state of the beam; thus, throughout the run, the controller strives to keep the beam in a roughly straight position.

Because the simulator described in chapter 4 was designed based on the particular configuration of the prototype beam used in the experimental tests, not many changes in implementation are required in moving from the simulations to the experiments. Thus, the implementation of both the modal and local controllers is kept essentially the same. The only major difference is that the optimal control gains are not obtained via numerical optimization, as in simulation, but rather picked by hand.[1]

The results of the experimental tests performed on the prototype beam are as follows. The experimentally measured buckling load of the beam is 5.3 Newtons. Under modal control, the maximum sustainable load is 19.4 Newtons, or 3.7 times the buckling load. The local controller performs slightly worse, with the maximum load of 16.8 Newtons, or 3.2 times the buckling load. In both cases, the sampling frequency of the controller is 3.8 kHz, which is the maximum frequency possible given the hardware at hand.

[1]The process of numerical optimization on the actual beam requires constant human intervention in order to continuously restart the experiment (by positioning the beam, as described above) given a new set of control gains. Manual tuning of the gains turned out to be easier to carry out.

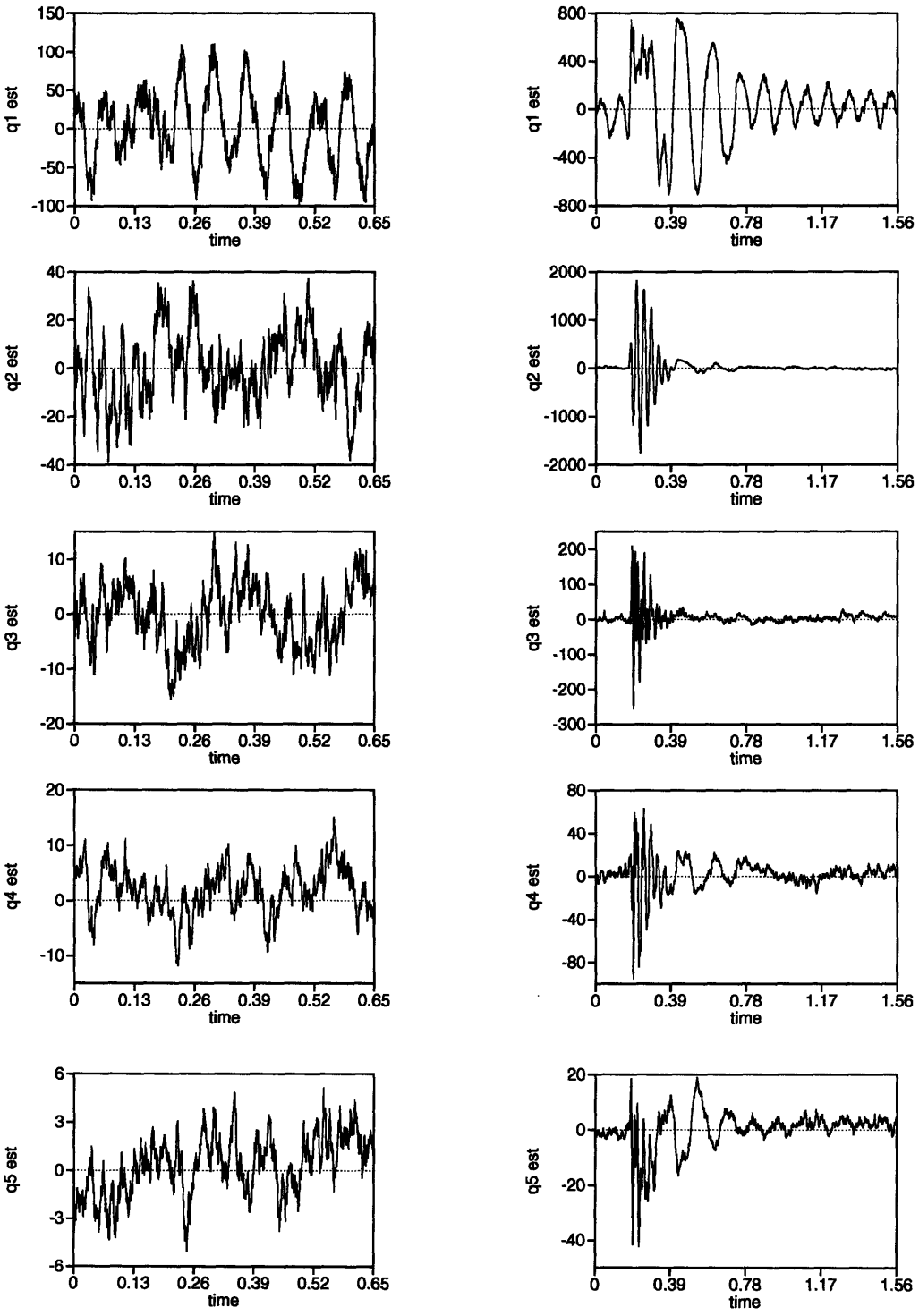

Figure 5-1: Modal amplitude estimates $\hat{q}_1, \ldots, \hat{q}_5$ of the prototype beam (a) during normal operation, and (b) during and after a disturbance. The beam is subjected to a compressive load of 14.4 Newtons, and is controlled by the modal controller.

Figure 5-1 demonstrates the performance of the prototype beam under modal control (similar plots would be obtained for the case of local control). In this example, the compressive load placed on the beam is approximately 14.4 Newtons. In figure 5-1a, the estimates of modal amplitudes $\hat{q}_1(t), \ldots, \hat{q}_5(t)$ are shown for the duration of 0.65 seconds during the beam's normal operation. Unlike in simulation, in reality the beam is never perfectly stabilized: the modal amplitudes oscillate slightly in response to measurement noise and small disturbances to the system. Notice that the average values of the modal amplitude peaks decrease with the mode number, as expected. This confirms the qualitative result obtained in chapter 3: higher modes are more difficult to excite, and thus on the average have smaller amplitudes.

Figure 5-1b shows what happens when the system is subjected to a significant disturbance. In this case, the disturbance is created by banging a fist on the table which is used to support the experimental apparatus. The modal amplitude estimates $\hat{q}_1(t), \ldots, \hat{q}_5(t)$ are plotted in the figure during and after the disturbance. The excitation of the system results in large oscillations exhibited in the modal response, which decay over time after the disturbance is removed. As in figure 5-1a, the amplitude of the oscillations generally decreases with the mode number. Notice however that in this case, mode 2 is excited more than any other mode; this is probably because the banging occurred at (or close to) the resonant frequency of mode 2.

5.2 Discussion

How does the performance of the prototype beam under modal and local control compare to the performance predicted through qualitative analysis and simulation?

The simulation results presented in chapter 4 (and compared against the experimental data in table 5.1) indicate that the local controller performs slightly worse than the modal controller at the sampling frequency of 3.8 kHz: the maximum sustainable load under local control is 4.0 times the buckling load of the simulated beam, versus the maximum load of 4.1 times the buckling load under modal control. This result is qualitatively confirmed by the analysis of chapter 3, which predicts the level of performance for local control to be almost as good as that achieved by the modal controller. The experimental figures of 3.7 and 3.2 times the buckling load for modal and local control, respectively, agree with this prediction as well. The figures 3.7 and 3.2 are lower than the values 4.1 and 4.0 obtained in simulation, which is to be expected when comparing the real system with a simulated version of it.

Note, however, that the value of the buckling load obtained for the simulated beam—namely, 1.5 Newtons—does not correspond to the experimentally measured value of 5.3 Newtons. As a result, the maximum weights supported by the prototype beam under modal and local control (19.4 and 16.8 Newtons, respectively) are much greater than the maximum sustainable loads predicted in simulation (6.2 and 6.1 Newtons for modal and local control, respectively). The most likely major reason for this discrepancy is the fact that we neglected the effects of sensors and actuators when modeling the material properties of the beam. Because sensing and actuation devices mounted on the surface of the beam modify the effective mass and stiffness

	max load / buckling load	
	modal control	local control
simulation	4.1	4.0
experiment	3.7	3.2

Table 5.1: Summary of system performance under modal and local control: simulation results vs. experimental results. Maximum sustainable load for modal and local control is specified as a ratio to the buckling load. The sampling rate of the controller is 3.8 kHz.

of the column, the value for the buckling load is also affected. In a more accurate simulation, a more sophisticated finite element model would account for the effects of the active control components on the material properties of each segment of the beam.

Further discrepancies between the simulated and the experimental results can be explained by various imperfections in the real system. For example, the piezo-ceramic actuators used in the experiments do not always behave in a linear fashion; e.g., they exhibit hysteresis, as described in [7, pp. 39–40]. Other nonlinearities are inherent in the dynamics of the beam itself; the linear model of the system employed in the simulations does not take these nonlinearities into account.

All in all, the prototype beam performs rather well given the imperfections in the real system, the small sampling rate of the controllers, and the relatively poor quality of sensors and actuators. In the future, we can expect the quality of active control components (including sensors, actuators, and computational elements) to be improved, yielding buckling control systems with even better performance.

Chapter 6

Conclusion

6.1 Summary

This thesis investigates techniques for active buckling control of a compressively-loaded structural element. Buckling is an important phenomenon limiting the load-bearing strength of a structure. Active control of buckling makes it possible to increase the load-bearing capabilities of compressive members, leading to structures that are both stronger and lighter than the passive structures built today.

In this thesis, we examined two different approaches to active buckling control. Modal control is an example of a centralized control strategy: it uses a global model of the system to be controlled (namely, the modal representation of the system dynamics), as well as global sensor information, to calculate control actions. In contrast, local control is decentralized: the control actions are computed based on local sensor information, and no global model of the system is employed. While Berlin in [7] used modal control methods to perform active control of a buckling beam, we are not aware of any previous work regarding decentralized approaches to buckling control.

In order to compare the relative performance of the modal and local control strategies, we conducted qualitative analysis, simulation, and experimentation on a prototype beam. In all cases, the results indicate that the local controller is capable of increasing the load-bearing strength of the beam to levels almost as high as those achieved through the use of modal control. Furthermore, because the local controller operates strictly on the basis of local sensor measurements, it is much easier to implement than the modal controller, which must constantly convert between the physical representation of sensor readings and actuator forces, and the modal representation used by the control law, subject to such phenomena as observation and control spillover. In addition, a practical implementation of local control may employ multiple computational units to handle control of small local regions of the structure, simplifying the tasks of data collection, processing, and distribution.

In spite of the efficiency and simplicity of local control, the higher performance levels achieved by the modal controller may still make centralized control the methodology of choice for simple structures such as beams. However, the real motivation behind the research described in this thesis is to develop techniques for buckling control

of large, complex structures which require many sensing sites and are characterized by interactions between members that are difficult to model accurately on a global scale. In these cases, centralized control techniques are much more difficult (if not impossible) to apply, and decentralized approaches become even more attractive.

In the long run, decentralized control of buckling has the potential to replace some of the strength and precision inherent in modern structures with intelligence, even in the cases when centralized control cannot be applied. For example, we can envision a portable bridge carried around in a vehicle that could be quickly installed on demand, or a tall building actively controlled to resist dynamic loads during an earthquake. The work presented in this thesis takes one of the first steps toward realizing these visions.

6.2 Future Work

Much work remains to be done before the long-term goals can become a reality. First of all, although our motivation for decentralized control has been its applicability to the control of large, complex structures, so far the local control strategy has only been tried on a simple structural element. Future work in active buckling control would include testing the local controller on composite structures with many structural members. For example, in [7], Berlin constructed a railroad-style truss bridge with two compressive members, and used a modal controller to successfully stabilize each of the members. The local controller developed in this thesis should be applied to this and other more complex structures in order to further investigate the feasibility of the purely local approach.

It might well turn out that more complex structures cannot be effectively controlled using purely local control techniques. This will prompt the development of more sophisticated decentralized strategies for active buckling control. One possibility would be to employ hierarchies of controllers, in the spirit of the hierarchic control architecture of Hall et al. ([13], [15]) mentioned in chapter 1. The controllers at each level in the hierarchy would base their actions on the aggregates of the state information obtained by the level below. Thus, the lowest level of the hierarchy would implement purely local control, while the highest level would have access to the aggregates of all available state information. The controllers at the higher levels in the hierarchy would act to control those global motions of the structure which could not be effectively influenced via local control.

Another important problem that has not been addressed as part of this work is the development of *adaptive* control strategies for active buckling control. As they stand now, both of the controllers implemented in this thesis are tuned (via adjustment of the control gains) to accommodate the prespecified static load; significant changes in the compressive load would require changes in the gains of the control laws, and are thus not tolerated well. More sophisticated adaptive control methods would be able to support dynamic loads, and adapt to other changes in environmental conditions. This ability of the system to accommodate the changes in its environment will be essential for future applications of active buckling control.

Bibliography

[1] Thomas Bailey and James E. Hubbard Jr., "Distributed Piezoelectric-Polymer Active Vibration Control of a Cantilever Beam," *Journal of Guidance and Control*, Vol. 8, No. 5, pp. 605–11, September–October 1985.

[2] Mark J. Balas, "Feedback Control of Flexible Systems," *IEEE Transactions on Automatic Control*, Vol. AC-23, No. 4, pp. 673–9, August 1978.

[3] Mark J. Balas, "Trends in Large Space Structure Control Theory: Fondest Hopes, Wildest Dreams," *IEEE Transactions on Automatic Control*, Vol. AC-27, No. 3, pp. 522-34, June 1982.

[4] Klaus-Jürgen Bathe and Edward L. Wilson, *Numerical Methods in Finite Element Analysis*, Prentice Hall, New Jersey, 1976.

[5] A. Baz, S. Poh, and P. Studer, "Modified Independent Modal Space Control Method for Active Control of Flexible Systems," *Proceedings of the VPI/AIAA Symposium on the Dynamics and Control of Large Flexible Spacecraft*, pp. 477–93, 1987.

[6] W. H. Bennett and R. E. Lindberg, "Decentralized Control Design for Large Flexible Spacecraft," *Dynamics and Control of Large Space Structures, Proceedings of the 4th VPI and SU/AIAA Symposium*, Meirovitch, L. (ed.), Blacksburg, VA, June 1983.

[7] Andrew A. Berlin, *Towards Intelligent Structures: Active Control of Buckling*, PhD Thesis, Department of Electrical Engineering and Computer Science, Massachusetts Institute of Technology, May 1994.

[8] *The Boston Globe*, "Accident Closes Part Of Major Artery; Jams Morning Commute," by John J. Mullins, Thursday, May 2, 1996.

[9] Shawn E. Burke and James E. Hubbard, Jr., "Active Vibration Control of a Simply Supported Beam Using a Spatially Distributed Actuator," *IEEE Control Systems Magazine*, Vol. 7, No. 4, pp. 25–30, August 1987.

[10] T. D. Burton, *Introduction to Dynamic Systems Analysis*, McGraw-Hill, Inc., 1994.

[11] Stephen H. Crandall, Norman C. Dahl, and Thomas J. Lardner, *An Introduction to the Mechanics of Solids*, 2nd edition with SI units, McGraw-Hill, Inc., 1978.

[12] Edward J. Davison, "The Robust Decentralized Control of a General Servomechanism Problem," *IEEE Transactions on Automatic Control*, Vol. AC-21, No. 1, pp. 14–24, February 1976.

[13] Steven R. Hall, Edward F. Crawley, Jonathan P. How, and Benjamin Ward, "Hierarchic Control Architecture for Intelligent Structures," *Journal of Guidance, Control, and Dynamics*, Vol. 14, No. 3, pp. 503–12, May–June 1991.

[14] J. P. Den Hartog, *Strength of Materials*, McGraw-Hill, Inc., 1949.

[15] Jonathan P. How and Steven R. Hall, "Local Control Design Methodologies for a Hierarchic Control Architecture," *Journal of Guidance, Control, and Dynamics*, Vol. 15, No. 3, pp. 654–63, May–June 1992.

[16] Altuğ İftar and Ümit Özgüner, "Local LQG/LTR Controller Design for Decentralized Systems," *IEEE Transactions on Automatic Control*, Vol. AC-32, No. 10, pp. 926–30, October 1987.

[17] Daniel J. Inman, *Engineering Vibration*, Prentice Hall, New Jersey, 1994.

[18] M. L. James et al., *Vibration of Mechanical and Structural Systems*, 2nd edition, Harper Collins College Publishers, 1994.

[19] Benjamin C. Kuo, *Automatic Control Systems*, 7th edition, Prentice Hall, New Jersey, 1995.

[20] Harry Y-F. Lam, *Analog and Digital Filters: Design and Realization*, Prentice-Hall, Inc., New Jersey, 1979.

[21] *Matlab User's Guide: High-Performance Numeric Computation and Visualization Software*, The Math Works, Inc., August 1992.

[22] L. Meirovitch, H. Baruh, and H. Öz, "A Comparison of Control Techniques for Large Flexible Systems," it Journal of Guidance and Control, Vol. 6, No. 4, pp. 302–10, August 1983.

[23] Katsuhiko Ogata, *Modern Control Engineering*, 2nd edition, Prentice Hall, New Jersey, 1990.

[24] Alan V. Oppenheim and Ronald W. Schafer, *Discrete-Time Signal Processing*, Prentice Hall, New Jersey, 1989.

[25] William J. Palm III, *Modeling, Analysis, and Control of Dynamic Systems*, John Wiley & Sons, 1983.

[26] Mario Paz, *Structural Dynamics Theory and Computation*, 3rd edition, Van Nostrand Reinhold, New York, 1991.

[27] F. M. Pitman and M. Ahmadian, "Decentralized Control of Large-Scale Systems," *Dynamics and Control of Large Space Structures, Proceedings of the 6th VPI and SU/AIAA Symposium*, Meirovitch, L. (ed.), Blacksburg, VA, pp. 103–15, July 1987.

[28] William H. Press, Saul A. Teukolsky, William T. Vetterling, and Brian P. Flannery, *Numerical Recipes in C: The Art of Scientific Computing*, 2nd edition, Cambridge University Press, 1992.

[29] Helen A. Ryaciotaki-Boussalis and Shyh Jong Wang, "A Decentralized Approach to Vibration Suppression in Segmented Reflector Telescopes," *Proceedings of the 1989 American Control Conference*, Pittsburgh, PA, Institute of Electrical and Electronics Engineers, Piscataway, NJ, pp. 2548–53, June 1989.

[30] Nils R. Sandell, Jr., Pravin Varaiya, Michael Athans, and Michael G. Safonov, "Survey of Decentralized Control Methods for Large Scale Systems," *IEEE Transactions on Automatic Control*, Vol. AC-23, No. 2, pp. 108–28, April 1978.

[31] Bernd E. Schäfer and Hans Holzach, "Experimental Research on Flexible Beam Modal Control," *Journal of Guidance and Control*, Vol. 8, No. 5, pp. 597–604, September–October 1985.

[32] Larry Silverberg, "Uniform Damping Control of Spacecraft," *Journal of Guidance, Control, and Dynamics*, Vol. 9, No. 2, pp. 221–7, March–April 1986.

[33] T. T. Soong, *Active Structural Control: Theory and Practice*, Longman Scientific & Technical, copublished with John Wiley & Sons, New York, 1990.

[34] Stephen P. Timoshenko and James M. Gere, *Mechanics of Materials*, D. Van Nostrand Company, 1972.

[35] S. Timoshenko et al., *Vibration Problems in Engineering*, 4th edition, Jon Wiley & Sons, 1974.

[36] Shih-Ho Wang and Edward J. Davison, "On the Stabilization of Decentralized Control Systems," *IEEE Transactions on Automatic Control*, Vol. AC-18, No. 5, pp. 473–8, October 1973.

[37] George S. West-Vukovich, Edward J. Davison, and Peter C. Hughes, "The Decentralized Control of Large Flexible Space Structures," *IEEE Transactions on Automatic Control*, Vol. AC-29, No. 10, pp. 866–79, October 1984.

[38] K. D. Young, "An Application of Decomposition Techniques to Control of Large Structures," *Dynamics and Control of Large Space Structures, Proceedings of the 4th VPI and SU/AIAA Symposium*, Meirovitch, L. (ed.), Blacksburg, VA, June 1983.

[39] W. Zuk and R. Clark, *Kinetic Architecture*, Van Nostrand Reinhold Company, New York, 1970.